AD-A049 144 NAVAL POSTGRADUATE SCHOOL MONTEREY CALIF F/G 8/10
ATMOSPHERIC TURBULENCE MEASUREMENTS IN MARINE FOG DURING CEWCOM--ETC(U)
DEC 77 C W FAIRALL, K L DAVIDSON
UNCLASSIFIED NPS61-77-004 NL

| OF |
AD
A049144

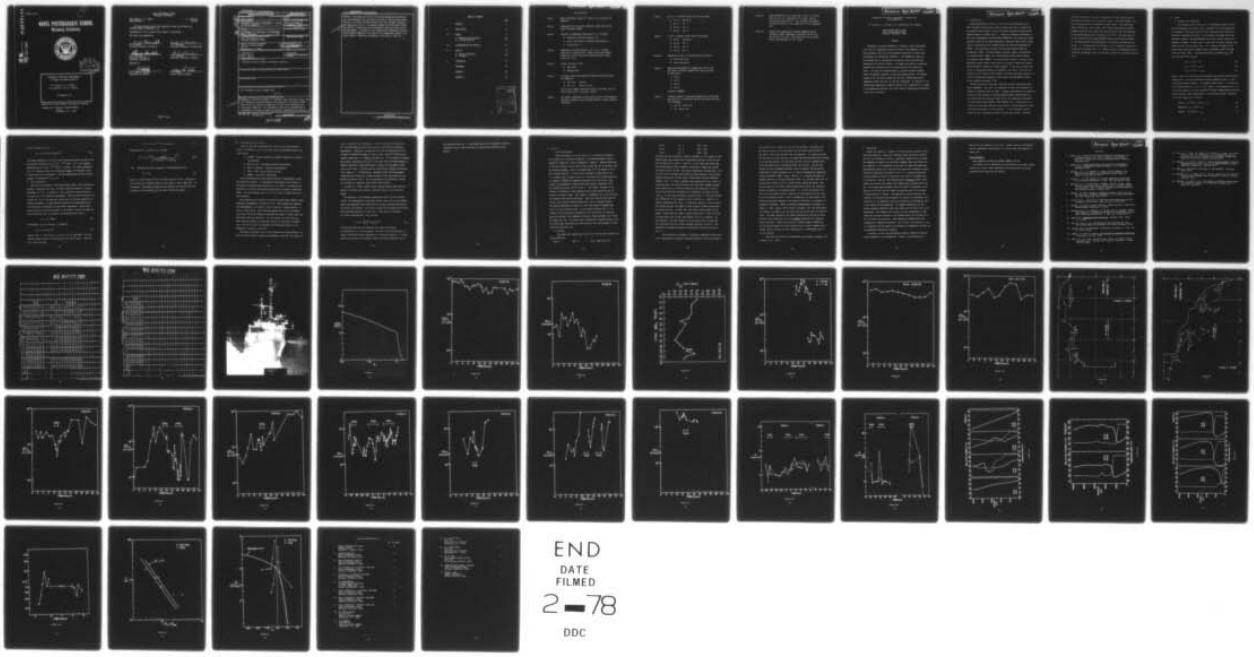

END
DATE
FILMED
2-78
DDC

AD A049144

AD No. ____
DDC FILE COPY

NPS61-77-004

NAVAL POSTGRADUATE SCHOOL
Monterey, California

DDC
RECEIVED
JAN 31 1978
A

ATMOSPHERIC TURBULENCE MEASUREMENTS
IN MARINE FOG DURING CEWCOM-76

C.W. Fairall, K.L. Davidson,
T.M. Houlihan, and G.E. Schacher

29 December 1977

Approved for public release; distribution unlimited

Prepared for: Naval Air Systems Command
R 370
Washington, D.C. 20360

NAVAL POSTGRADUATE SCHOOL
Monterey, California

Rear Admiral I. W. Linder
Superintendent

J. R. Borsting
Provost

The work reported herein was supported in part by the Naval Air Systems Command, Washington, D.C.

Reproduction of all or part of this report is authorized.

The report was prepared by:

C. W. Fairall
Assistant Professor of Physics

K. L. Davidson
Associate Professor of Meteorology

T. M. Houlihan
Associate Professor of
Mechanical Engineering

G. E. Schacher
Associate Professor of Physics

Approved by:

K. E. Woehler, Chairman
Department of Physics

W. M. Tolles
Acting Dean of Research

NPS61-77-004

UNCLASSIFIED
SECURITY CLASSIFICATION OF THIS PAGE (When Data Entered)

REPORT DOCUMENTATION PAGE

READ INSTRUCTIONS BEFORE COMPLETING FORM

1. REPORT NUMBER: NPS61-77-004	2. GOVT ACCESSION NO.
3. RECIPIENT'S CATALOG NUMBER	
4. TITLE (and Subtitle): Atmospheric Turbulence Measurements in Marine Fog during CEWCOM-76	5. TYPE OF REPORT & PERIOD COVERED: Technical Report.
	6. PERFORMING ORG. REPORT NUMBER
7. AUTHOR(s): C.W. Fairall, K.L. Davidson, T.M. Houlihan and G.E. Schacher.	8. CONTRACT OR GRANT NUMBER(s)
9. PERFORMING ORGANIZATION NAME AND ADDRESS: Naval Postgraduate School, Monterey, California 93940	10. PROGRAM ELEMENT, PROJECT, TASK AREA & WORK UNIT NUMBERS
11. CONTROLLING OFFICE NAME AND ADDRESS: Naval Air Systems Command, AIR 370, Washington, D.C. 20360	12. REPORT DATE: 29 December 1977 13. NUMBER OF PAGES: 53
14. MONITORING AGENCY NAME & ADDRESS (if different from Controlling Office): 59 p.	15. SECURITY CLASS. (of this report): Unclassified 15a. DECLASSIFICATION/DOWNGRADING SCHEDULE

16. DISTRIBUTION STATEMENT (of this Report)

Approved for public release; distribution unlimited.

17. DISTRIBUTION STATEMENT (of the abstract entered in Block 20, if different from Report)

18. SUPPLEMENTARY NOTES

19. KEY WORDS (Continue on reverse side if necessary and identify by block number)

Fog, turbulence, marine boundary layer

epsilon

20. ABSTRACT (Continue on reverse side if necessary and identify by block number)

Atmospheric turbulence parameters ε (turbulent energy dissipation rate), and C_T^2 (temperature structure function) were measured in the marine boundary layer during the Cooperative Experiment for West Coast Oceanography and Meteorology (CEWCOM-76). The atmospheric stability was characterized by measurements of profiles of mean wind velocity, temperature and relative

C sub T squared

(over)

DD FORM 1 JAN 73 1473 EDITION OF 1 NOV 65 IS OBSOLETE
S/N 0102-014-6601

UNCLASSIFIED
SECURITY CLASSIFICATION OF THIS PAGE (When Data Entered)

251 450

humidity. This paper will focus on turbulence properties and turbulent heat flux measured during four marine fog events. The fogs were characterized by a slightly unstable boundary layer with moderate increases of heat flux during the fog. An ensemble average of the fog events showed that C_T^2 and ε reached peak values immediately before and after the fog was encountered. An analysis of the dimensionless temperature structure function (C_T^2 normalized by the square of the temperature gradient) gave lower values of temperature fluctuations in fog than in clear air.

TABLE OF CONTENTS

ACCESSION for
NTIS White Section
DDC Buff Section
UNANNOUNCED
JUSTIFICATION
BY
DISTRIBUTION/AVAILABILITY CODES
Dist. AVAIL. and/or SPECIAL
A

Preceding Page Blank FILMED

Figure Captions

Figure 1 Naval Postgraduate School R/V Acania at the conclusion of CEWCOM-76.

Figure 2 Normalized heat conduction coefficient (eddy diffusivity) versus Richardson number.

Figure 3 Variation of atmospheric quantities at Z = 10 meters:

a) temperature structure function, C_T^2

b) rate of dissipation of velocity fluctuations, ε

c) wind velocity, U

Figure 4 Temperature structure function, C_T^2, at Z = 10 meters versus time in Monterey Bay. Solid circles are unstable conditions (12/76) and solid triangles are near neutral conditions (7/76).

Figure 5 Diurnal variation of C_T^2:

a) open ocean

b) coastal ocean

Figure 6 R/V Acania tracks off Southern California during fog events for CEWCOM-76:

a) Sep 27-29 (Fog #1)

b) Oct 5-9 (Fog #'s 2,3,4)

The six digit number indicates the day of the month (dd) and time of day (tttt) in the code - ddtttt.

Figure 7 Sea surface temperature contours from aircraft IR measurements. Courtesy of Backes (1977) and Ralph Markson, Airborne Research Associates.

Figure 8 C_T^2 at Z = 10 meters versus time for fog events:

a) Fog #1 Sep 27-28

b) Fog #2 Oct 5

c) Fog #3 Oct 8

d) Fog #4 Oct 9

Figure 9 ε at Z = 10 meters versus time for fog events:

a) Fog #1 Sep 27-28

b) Fog #2 Oct 5

c) Fog #3 Oct 8

d) Fog #4 Oct 9

Figure 10 Sensible heat flux, W, versus time for fog events:

a) Fog #1 and Fog #2

b) Fog #3 and Fog #4

Figure 11 Radiosonde measurements of temperature (solid line) and relative humidity (dashed line) versus altitude for fog events:

a) Fog #1

b) Fog #2

c) Fog #3

d) Fog #4

Courtesy of NWSMET.

Figure 12 Ensemble average of turbulence parameters one hour before and after fog is encountered and one hour before and after fog dissipates:

a) $C_T^2/\overline{C_T^2}$ versus time

b) $\varepsilon/\overline{\varepsilon}$ versus time

Figure 13 Height dependence of C_T^2 normalized to the Z = 6.6 meter value for fog (x's) and non-fog (o's) data. Neutral equilibrium yields the $Z^{-2/3}$ line indicated, non-neutral equilibrium would be a less steep line in this representation.

Figure 14 Dimensionless temperature structure parameter versus Richardson number (atmospheric stability) for fog (x's) and non-fog (o's) data. The solid line is the overland results from Wyngaard, et. al. (1971).

Preceding Page BLANK - NOT FILMED

Atmospheric Turbulence Measurements in Marine Fog during CEWCOM-76

C.W. Fairall, K.L. Davidson, T.M. Houlihan and G.E. Schacher

Environmental Physics Group
Naval Postgraduate School
Monterey, California 93940

Abstract

Atmospheric turbulence parameters ε (turbulent energy dissipation rate), and C_T^2 (temperature structure function) were measured in the marine boundary layer during the Cooperative Experiment for West Coast Oceanography and Meteorology (CEWCOM-76). The atmospheric stability was characterized by measurements of profiles of mean wind velocity, temperature and relative humidity. This paper will focus on turbulence properties and turbulent heat flux measured during four marine fog events. The fogs were characterized by a slightly unstable boundary layer with moderate increases of heat flux during the fog. An ensemble average of the fog events showed that C_T^2 and ε reached peak values immediately before and after the fog was encountered. An analysis of the dimensionless temperature structure function (C_T^2 normalized by the square of the temperature gradient) gave lower values of temperature fluctuations in fog than in clear air.

Preceding Page BLANK - NOT FILMED

I. Introduction

During September and October of 1976 the Naval Postgraduate School (NPS) shipboard turbulence and profile systems were used in a marine fog and boundary layer research cruise off Southern California aboard the NPS research vessel R/V ACANIA (Fig. 1). Termed the Cooperative Experiment in West Coast Oceanography and Meteorology (CEWCOM-76), the cruise was jointly organized by NPS and the Naval Electronics Laboratory Center (NELC) of San Diego in collaboration with CALSPAN Corporation under the sponsorship of NAVAIR. Also represented on board were the Naval Avionics Facility, Indianapolis (NAFI), the Naval Research Laboratory (NRL), the California Air Resources Board (CARB), and a Naval Weather Systems Service Mobile Environmental Team (NWSMET). This was the most recent of a series of data gathering cruises forming a major part of a program of marine fog investigation sponsored by Naval Air Systems Command. It was also the third such cruise to include measurements of atmospheric turbulence. The first was conducted in 1974 aboard the R/V ACANIA off Northern California (Mack et al, 1975); the second was conducted in 1975 aboard the USNS HAYES off Novia Scotia (Gathman and Larson, 1976).

Marine fog is one of the least understood and most complicated atmospheric phenomena. Mack (1975) has identified at least five different fog formation "scenarios" over the ocean. Although considerable fog forecasting success has been obtained by skilled phenomenologists employing various fog indices (such as inversion height and air sea temperature difference) in local coastal areas (Leipper, 1948. Backes, 1977), accurate marine fog prediction in the open ocean will surely benefit from applications of knowledge from the synoptic to the microscale. On the microscale, the production of fog is governed by several (interacting) factors: aerosols,

radiation, hydrostatic stability, temperature inversion characteristics, and turbulent transport of heat and water vapor. Turbulent transport was first incorporated into fog modeling by Rodhe (1962). More modern fog models (Lee and Lin, 1975; Barker, 1975) employ sophisticated turbulent parameter stability and scaling laws (see section II) that are unverified in the marine boundary layer (Davidson et al, 1977). The main thrust of the NPS turbulence group during CEWCOM-76 was to attack these problems by: 1) providing modelers with measurements of turbulence and mean profiles in fog, 2) obtaining data for evaluation of the turbulence scaling laws in the marine boundary layer, 3) examining some of the characteristics of turbulence "background" levels for non-fog conditions in the marine boundary layer.

II. Theory

A. Boundary layer equations

The boundary layer is that part of the atmosphere where friction with and heating by the surface play an important role in the generation of turbulence. Near the surface the shear stress and scalar fluxes are essentially constant with height. In this region the fluxes can be represented in terms of scaling parameters (such as u_* and T_*) that are independent of height. We shall refer to this layer of nearly constant shear stress and flux as the surface layer. For a complete treatment of the surface layer equations we suggest Lumley and Panofsky (1964), Businger (1971) and Kraus (1972). The normalized fluxes of momentum (F_m), heat (F_h) and water vapor (F_q) are

$$F_m = -\langle u'w' \rangle = u_*^2 \tag{1a}$$

$$F_h = -\langle T'w' \rangle = u_* T_* \tag{1b}$$

$$F_q = -\langle q'w' \rangle = u_* q_* \tag{1c}$$

where u' and w' are the fluctuating horizontal and vertical wind velocities, respectively, T' is the fluctuating potential temperature and q' is the fluctuating specific humidity. The Reynolds shear stress, τ, is related to the friction velocity, u_*, by $\tau = \rho u_*^2$, where ρ is the density of air. In the surface layer we can write simplified turbulent energy balance equations using production terms (proportional to the vertical gradient, $\partial X/\partial Z$) and dissipation terms [ε_x] as follows:

$$\text{velocity:} \quad u_*^2 \, \partial u/\partial z - \frac{g}{T} u_* T_{v*} = \varepsilon \tag{2a}$$

$$\text{temperature:} \quad u_* T_* \, \partial T/\partial z = \varepsilon_T \tag{2b}$$

$$\text{humidity:} \quad u_* q_* \, \partial q/\partial z = \varepsilon_q \tag{2c}$$

Note that the velocity equation (where $\varepsilon_u \equiv \varepsilon$) has an extra production (or suppression) term due to the bouyancy of air (T_v is the virtual potential temperature). In the surface layer, the appropriate turbulent transport scale parameter is the height above the surface, z. In this regime, turbulence properties can be scaled through the similarity parameter z/L, where L is the Monin-Obukhov stability length.

$$L = \frac{T\, u_*^2}{\kappa g\, T_{v*}}, \tag{3}$$

where $\kappa = .35$ is the von Karmon constant. We can now define the mean profile functions $\phi_x\ (z/L)$ as (Businger,et al, 1971)

$$\phi_x\ (z/L) = \frac{\kappa z}{x_*} \frac{\partial x}{\partial z} \tag{4}$$

If we define a dimensionless dissipation function (Wyngaard and Cote, 1971)

$$E_x\ (z/L) \equiv \frac{\varepsilon_x\, \kappa z}{u_*\, x_*^2} \tag{5}$$

then the energy equations become

$$\phi_u\ (z/L) - z/L = E_u\ (z/L) \tag{6a}$$

$$\phi_T\ (z/L) = E_T\ (z/L) \tag{6b}$$

$$\phi_q\ (z/L) = E_q\ (z/L) \tag{6c}$$

Present estimates of ϕ_x and E_u are given in Appendix A.

In the inertial subrange, turbulence is nearly isotropic and we can represent the intensity of turbulence fluctuations as a one-dimensional power spectrum, $S_x(k)$, of the form proposed by Kolmogorov

$$S_x(k) = .25\, C_x^2\, k^{-5/3} \tag{7}$$

where k is the wavenumber and C_x^2 is the structure function. If the quantity x has value x(r) at position r and value x(r + d) at position r + d then

$$C_x^2 = \langle [\, x(r) - x(r + d)]^2 \rangle \, d^{-2/3} \tag{8}$$

In the inertial subrange C_x^2 is independent of d. Corrsin (1951) has shown that the structure function can be related to the dissipation by

$$C_x^2 = 4 \, \beta_x \, \varepsilon^{-1/3} \, \varepsilon_x \tag{9}$$

where β_x is a constant, $\beta_T = \beta_q = .81$ and $\beta_u = .52$. We can construct a dimensionless temperature structure parameter, f(z/L), by combining eqs. 6 and 9 (Wyngaard, et al., 1971)

$$C_T^2 = T_*^2 \, z^{-2/3} \, f_1(z/L) \tag{10}$$

or, using eq. 4

$$C_T^2 = (\partial T/\partial z)^2 \, z^{4/3} \, f_2(z/L) \tag{11}$$

We can also use eq. 5 to obtain a similar expression for ε.

$$\varepsilon = \frac{u_*^3}{kz} \, E_u(z/L) \tag{12}$$

Since the Monin-Obukhov length is difficult to measure, we normally use an alternate stability variable-the gradient Richardson number, R_i,

$$R_i = \frac{g}{T} \frac{(\partial T_v/\partial z)}{(\partial u/\partial z)^2} \tag{13}$$

which is related to z/L by

$$R_i = (z/L)\ \phi_T(z/L)/(\phi_u(z/L))^2 \qquad (14)$$

The height dependence of C_T^2 and ϵ can be obtained from eqs. 10 and 12; for near neutral conditions ($R_i \simeq 0$) $C_T^2 \sim z^{-2/3}$ and $\epsilon \sim z^{-1}$. For unstable conditions ($R_i << 0$) $C_T^2 \sim z^{-4/3}$ and $\epsilon \sim$ constant. For stable conditions ($R_i > 0$), turbulent eddies are increasingly damped by increasing stable stratification of the atmosphere. Overland measurements indicate complete damping of turbulence for $R_i \geq .21$.

B. Flux calculations

There are four methods of calculating scalar fluxes: eddy correlation, gradient, turbulence, and bulk. The eddy correlation method is a direct measurement of $x'w'$ in equation 1. This requires a stable platform so we cannot use it for shipboard measurements. The bulk method (Friehe, 1977) relates the flux to the mean wind velocity and the air-sea temperature or humidity difference. We have found this method to be unsatisfactory due to difficulties in measuring the sea surface temperature. The gradient method relates the vertical gradient of the scalar to the flux through the eddy diffusivity, K_x. For instance, the normalized heat flux is

$$F_h = - K_T\ (\partial T/\partial z) \qquad (15)$$

Unfortunately, K_T is a function of stability,

$$K_T = \kappa\ z\ u_*/\phi_T\ (z/L) \qquad (16)$$

shown in Fig. 2. Note that $K_T = 0$ for $R_i \geq .21$ in this model. The turbulence method is based on calculations of T_* from C_T^2 and ϵ. Combining eqs. 9 and 6b we find

$$T_*^2 = \kappa z C_T^2 \varepsilon^{1/3}/(3.2 u_* \phi_T(z/L)) \quad (17)$$

Substituting for u_* with eq. 12, we obtain

$$F_h = \pm C_T \varepsilon^{1/3} \left[\frac{(\kappa z)^{4/3}}{3.2 (E_u(z/L))^{1/3} \phi_T(z/L)} \right]^{1/2} \quad (18)$$

The sensible heat flux is related to the normalized flux by

$$W = C F_h \quad (19)$$

where $C = 1.3 \times 10^3$ joule/(°C m^3) is the heat capacity of air. Equations 15 and 18 have their analogous forms for calculation of water vapor flux. Unfortunately, instrumental limitations and problems (see Section III) have prevented us from measuring C_q^2 and $(\partial q/\partial z)$ during fog events.

III. Instrumentation and Analysis

Since the NPS work represented only a part of the total shipboard effort for CEWCOM-76, we will first list the key measurements made by the other groups:

1. CALSPAN - aerosol spectra and chemical composition, visibility and profiles.
2. NRL (R. Jeck) - Knollenberg aerosol spectrometer.
3. NAFI (J. Russell) - microwave refractometer.
4. CARB - ozone, carbon monoxide and NO_x.
5. NWSMET - twice daily radiosondes.

The NPS instrumentation was primarily devoted to measurement of mean and turbulence profiles. A comprehensive description of this system is the subject of another paper (Houlihan, et al., 1977). The profiles were measured at four fully instrumented levels plus a sea surface temperature sensor. The level heights were 4.2, 6.6, 11.3 and 17.7 meters above the mean waterline.

Mean temperature was measured with Hewlett-Packard Model HP2801A quartz oscillator thermometers, accurate to .01 °C. Mean humidity was measured with Hydrodynamic,Inc. Digital II type 15-1818 LiCl Dunmore sensors, accurate to about 3% RH. These humidity sensors have very slow response above about 95% RH and response variations from sensor to sensor make them unreliable under fog conditions. For this reason, we do not have fog event humidity profiles of sufficient accuracy to calculate the humidity flux. The wind velocity was measured with Thornthwaite Model 101 cup anemometers, accurate to about 5%.

Wind speed fluctuations (for ε) were measured with Thermo-Systems, Inc. Model TSI 1054B constant temperature anemometers using TSI 1210 probes with

6 mil. cylindrical hot-film sensors. The hot films were calibrated on a TSI 1125 Calibrator with the cables actually used during the shipboard measurements. Temperature fluctuations (for C_T^2) were measured with GTE Sylvania ac wheatstone bridges (3.0 kHz carrier) using TSI 1210-P.8 micro thermal probes with 2.5 μ diameter platinum wire. We had planned to measure water vapor fluctuations (for C_q^2) at one level using an Electro-Magnetics Research Corporation Lyman-alpha sensor, however this instrument failed early in the cruise. The mean data was continuously averaged and periodically logged by a microprocessor designated MIDAS (Microprogrammable Integrated Data Acquisition System) developed at NPS and adapted for the ACANIA by Plunkett (1977). The fluctuating data was amplified, filtered and recorded on a Honeywell Model 5600 FM tape recorder.

In addition, the NPS acoustic radar (Aeroenvironment Model 300) was mounted on the ship and provided a continuous monitor of the inversion height.

The analysis of the turbulence signals was guided by noise considerations. The combination of long sensor cables (about 150 ft) and somewhat impure ship generated power restricted our analysis options--particularly for the hot film systems. The velocity signals were processed with Fourier power spectrum analyzers to yield $S_u(f)$. Using Taylor's hypothesis ($k = 2\pi f/u$) and equations 7 and 9 we find

$$\varepsilon = 2.67 \left(\frac{2\pi}{u}\right)^{3/2} \left[f^{5/3} S_u(f)\right]^{3/2} \qquad (20)$$

The spectral method has the advantage that power source noise (60,120,180 Hz, etc.) can be ignored. The bulk of the C_T^2 data were obtained from paired sensors (separated by 0.3 meters) using eq. 8. In some cases only one sensor was operable; these were spectrum analyzed and C_T^2

was calculated using eq. 7. Being based upon the high frequency turbulence components, both of these techniques are relatively unaffected by ship motions.

IV. Results

A. General Background

Before plunging into the fog data, it is of interest to examine the variability of turbulence parameters in the marine boundary layer to establish a feeling for typical "background" behavior. Nominal variations of C_T^2 and ε during a 24 hour period (Fig. 3a and Fig. 3b) in the open ocean are relatively smooth. Since ε is proportional to u^3, we expect it to be more variable than C_T^2. A typical daily variation of wind velocity at $z = 10$ meters (u_{10}) is shown in Fig. 3c. Of course, C_T^2 is quite sensitive to changes in atmospheric temperature gradients as we can see in a comparison of measurements in Monterey Bay under neutral conditions (7/76) and unstable conditions (12/76) in Fig. 4. The diurnal variation of C_T^2 overland is dominated by solar heating of the surface during the day and radiative cooling at night. This leads to a maximum of C_T^2 in the afternoon and minimum around sunrise and sunset. Since the ocean has both high heat capacity and excellent thermal conductivity (due to turbulent mixing), the surface temperature is subject to only a few tenths of degrees modulation by solar heating cycles. In the slightly unstable ($R_i \cong -0.1$) boundary layer we typically encountered in the open ocean, we found that radiation cooling of the atmosphere produced a slight maximum of C_T^2 during the night (Fig. 5a). In coastal areas, influenced by land-sea breeze cycles, we found diurnal variations more characteristic (but less extreme) of those found over land (Fig. 5b).

B. Fog Data

This paper will concentrate on the first four fog events encountered during CEWCOM 76:

Fog #1	Sept. 27	1100 - 0800 (Sept. 28)

Fog #2	Oct. 5	0700 - 1100
Fog #3	Oct. 8	1000 - 1800
Fog #4	Oct. 9	0800 - 1200

Fog event data are provided in tables in Appendix B. The location of the ACANIA during these events can be established from Fig. 6a (Fog #1) and Fig. 6b (Fog #'s 2,3, and 4). Fog #'s 1,3, and 4 were open ocean fogs, all located west of Point Conception; Fog #2 was a coastal fog located just south of Palos Verdes. Sea surface temperature contours (Fig. 7) for the first week of October were measured by Ralph Markson in the Airborne Research Associate's aircraft using a Barnes PRT-5 infrared radiometer (Backes, 1977). In order to simplify the presentation of four levels of turbulence data, the values from each level have been averaged together after translation to a 10 meter equivalent value using eqs. 10 and 12. The 10 meter equivalent averages of the temperature structure function ($\langle C_T^2 \rangle_{10}$) for the four fog events are given in Fig. 8. Note the considerable variability of C_T^2 compared to Fig. 3a and Fig. 4. Figure 9 is a similar presentation for $\langle \varepsilon \rangle_{10}$. In some cases values of ε are not available during fog since the impact of water droplets causes a noise spike by cooling the film. In heavy fog, this effect totally masks the real signal. We were able to obtain ε values during Fog #'s 1 and 4 by using hot wires which, due to their much smaller size (4.5 μ diameter), are less affected. The heat fluxes for the fog events (Fig.s 10a and 10b) were calculated from the 10 meter averages using eqs. 15 and 18. Representative radiosonde dew point and temperature profiles are given in Fig. 11.

The correlation of changes in turbulence parameters and fog events can be highlighted by preparing "ensemble" averages of the fog encounters.

Each fog event was divided into four one hour sections: one before and one after the fog is first encountered, and one before and one after the fog clears (Fog #2 was excluded from this analysis). If a given fog event was less than two hours duration, the second and third sections were shortened to 1/2 the fog duration. Note that both C_T^2 and ε rise to a maximum about 30 minutes before fog is encountered (Figs. 12a and 12b). One can also examine the more fundamental behavior of C_T^2 in terms of fog and non-fog comparisons of height dependence (eq. 10) and the dimensionless temperature structure parameter (DTSP), $f_2(R_i)$, from eq. 11. Although the height dependence exhibits no obvious disimilarity (Fig. 13), the DTSP curve (Fig. 14) implies lower values of C_T^2 for a given $(\partial T/\partial z)$ during fog events. This is consistent with the lower fluxes obtained during fog by the turbulence method as compared to the gradient method. It is quite conceivable that this is an instrumental effect, caused by the accumulation of liquid water on the microthermal sensors. Such an accumulation, if large enough, could reduce the frequency response of the sensors sufficiently to attenuate the measured fluctuations. Based on laboratory measurements of frequency response in salt coated wires (Fairall & Schacher, 1977) one would expect this effect to be small until the water film was on the order of 30 microns thick. The rapid increase of C_T^2 before dissipation of fog and the rapid decrease after dissipation are in the <u>opposite</u> direction of an expected water film effect. Despite the scarcity of droplet impacts observed on the 130 micron diameter hot films (implying the 2.5 micron diameter microthermal sensors remained very dry) during Fog #2, a considerable drop in C_T^2 was measured.

Fog event data from other investigators can be found in Backes (1977) and Mack, et al. (1977).

V. Conclusions

Despite the efforts of a number of scientists during a month of shipboard data gathering, unequivocal statements about the nature of marine fog are still difficult to come by. Although it might be wise to resist the temptation to embark into arm waving arguments about the reasons for fog formation, it is interesting to note that the three open ocean fogs described were found in the vicinity of the cold water intrusion at Point Conception (upper left hand corner of Fig. 6). To describe these fogs as being formed by "warm air blowing over cold water" is probably much too optimistic, since all were characterized by unstable surface layers. Indeed, the vertical heat fluxes often dramatically increased during the fog. We can make some statements about the nature of turbulence in fog, keeping in mind that they are subject to questions about the influence of water droplets on sensors. The temperature structure function (and therefore the turbulent heat transport) was subject to considerably more variations in the atmospheric conditions conducive to fog formation than in the typical non-fog background. An ensemble analysis of C_T^2 and ε showed increased turbulence levels just before and just after the fog was encountered. This suggests that the fog is often superimposed on some large scale cellular structure in the boundary layer (on the order of 10 km in the down wind direction). When analyzed in dimensionless form (normalized by temperature gradient), C_T^2 is lower in fog than out of fog. It is possible the fog droplets are retarding the temperature fluctuations by evaporation-condensation response.

In general, we have made considerable progress towards the specific goals enumerated in the introduction. Notably in the provision of a

body of data for modelers to work with. However, there is considerable room for improvement (particularly in the water vapor flux capacity) in future work.

Acknowledgements

Work supported by Naval Air Systems Command, AIR 370

The authors wish to acknowledge the contributions of Lyn May, Charles Leonard, Ray Garcia, Captain Reynolds and the Acania crew, and cruise organizers Dale Leipper and Ted Calhoun.

Preceding Page BLANK - NOT FILMED

References

1. Backes, D.A., "Santa Ana associated offshore fog: forecasting with a sequential model", M.S. Thesis, (advisor, Dale Leipper), Report No. NPS-68Lr77091, Naval Postgraduate School, Monterey, California (1977).

2. Barker, E.H., "A maritime boundary layer model for the prediction of fog", ENVPREDRSCHFAC Technical Paper No. 4-75, Monterey, California (1975).

3. Businger, J.A., J.C. Wyngaard, Y. Izumi, and E.F. Bradley, "Flux profile relationships in the atmospheric surface layer", J. Atmos. Sci. 28, 181-189 (1971).

4. Corrsin, S., "On the spectrum of isotropic temperature fluctuations in an isotropic turbulence", J. Appl. Phys. 22, 469-473 (1951).

5. Davidson, K.L., T.M. Houlihan, G. Schacher, and C.W. Fairall, "Examination of turbulence scaling laws for C_T^2 in the layer adjacent to ocean waves", Proc. of Optical Propagation through Turbulence, Rain, and Fog, Boulder, Colorado (1977).

6. Fairall, C.W. and G. Schacher, "Frequency response of hot wires used for atmospheric turbulence measurements in the marine environment", Rev. Sci. Instrum. 47, 12-17 (1977).

7. Friehe, Carl A., "Estimation of refractive-index temperature structure parameter over the ocean", Appl. Opt. 16, 334-340 (1977).

8. Gathman, S.L. and R.E. Larson (Editors), "Marine fog cruise, USNS Hayes", NRL-ONR Report, Washington, DC (1976).

9. Houlihan, T.M., K.L. Davidson, C.W. Fairall, and G.E. Schacher, "Experiment aspects of a shipboard system used in investigations of over-water turbulence and profiles", J. Appl. Met. (submitted 1977).

10. Kraus, E.B., Atmosphere-Ocean Interaction, Clarendon Press, Oxford, Ch. 5 (1972).

11. Lee, S.C. and C.L. Lin, "An analytical study of marine fog", Proc. Third Annual Marine Fog Conference, San Diego, California (1975).

12. Leipper, Dale, "Fog development at San Diego, California", J. Mar. Res. 7, 337-346 (1948).

13. Lumley, J.L. and H.A. Panofsky, The Structure of Atmospheric Turbulence, Interscience, New York (1964).

14. Mack, E.J., R.J. Pilie, and Ulrich Katz, "Marine fog studies off the California Coast", Calspan Corp. Report No. CJ-5607-M-1, Buffalo, New York (1975).

15. Mack, E.J., U. Katz, C.W. Rogers, D.W. Gaucher, K.R. Piech, C.K. Akers, and R.J. Pilie, "An investigation of the meteorology, physics, and chemistry of marine boundary layer processes", Calspan Corp. Report No. CJ-6017-M-1, Buffalo, New York (1977).

16. Plunkett, J.R. and T.M. Houlihan, "MIDAS-a microprogrammable integrated data acquisition system", Proc. of the IEEE Conference on microcomputers, Oklahoma City, Oklahoma (1977).

17. Rodhe, B., "The effect of turbulence on fog formation", Tellus 24, 49-86 (1962).

18. Wyngaard, J.C., Y. Izumi, and S.A. Collins, "Behavior of the refractive index-structure parameter near the ground", J. Opt. Soc. Am. 61, 1646-1650 (1971).

19. Wyngaard, J.C. and O.R. Cote, "The budgets of turbulent kinetic energy and temperature variance in the atmospheric surface layer", J. Atmos. Scie. 28 (1971).

Appendix A

The forms of the mean profile functions are taken from Businger, et al (1971).

$$\phi_u(z/L) = (1 - 15\ z/L)^{-1/4} \qquad z/L < o$$

$$\phi_u(z/L) = (1 + 4.7\ z/L) \qquad z/L > o$$

$$\phi_T(z/L) = .74\ (1 - 9\ z/L)^{-1/2} \qquad z/L < o$$

$$\phi_T(z/L) = (.74 + 4.7\ z/L) \qquad z/L > o$$

The dimensionless velocity dissipation function is from Wyngaard and Cote (1971).

$$E_u(z/L) = [1 + .5|z/L|^{2/3}]^{3/2} \qquad z/L < o$$

$$E_u(z/L) = [1 + 2.5(z/L)^{3/5}]^{3/2} \qquad z/L > o$$

The dimensionless temperature structure functions is from Wyngaard, et al (1971).

$$f_1(z/L) = 4.9\ (1 - 7\ z/L)^{-2/3} \qquad z/L < o$$

$$f_1(z/L) = 4.9\ (1 + 2.75\ z/L) \qquad z/L > o$$

Appendix B

	Date	Start Time	End Time	T_s °C	T_{10} °C	U_{10} m/sec	$(\partial t/\partial z)_{10}$ 10^{-2} °c/m	U_* m/sec	R_{110}	C^2_{T10} 10^{-3} °c^2/m$^{4/3}$	ε_{10} 10^3 m^2/sec^3	grad W	turb watt/m^2	
Fog 1	9/27	1540	1611	17.91	17.64	3.4	-.44	.14	-.11	.40	.87	4.4	3.2	
		1637	1711	18.28	17.90	3.1	.14	.09	.057	1.40	.23	- .4	-3.2	Fog
		1713	1747	17.88	18.36	2.9	-.47	.11	-.14	.85	.43	3.9	3.6	Fog
		1749	1823	18.01	18.41	3.9	-.04	.12	-.02		.48	.3		Fog
		2048	2122	17.65	17.30	3.6	.41	.09	.25	.08	.22	0	0	
		2124	2158	17.72	17.54	3.8	.07	.09	.04	.05	.19	- .3	- .6	
		2200	2222	17.84	17.53	4.0	-.02	.10	-.01		.28	.1	1.2	
		2250	2312	17.78	17.36		-.13	.12	-.04	.09	.46	1.0	1.4	
		2334	2359	17.68	16.59		-.25	.12	-.07	.50	.51	2.0	3.0	Fog
	9/28	0010	0044	17.67	16.61		-.13	.11	-.05	.41	.33	.9	2.6	Fog
		0046	0126	17.68	16.70		-.04	.08	-.02	.22	.17	.2	1.8	Fog
		0145	0206	17.66	16.29		-.42	.12	-.12	.20	.49	3.3	2.0	Fog
		0209	0226	17.67	16.43		-.39	.12	-.11	.85	.56	3.2	4.0	Fog
		0245	0250	17.67	16.34		-.56	.12	0.16	.31	.44	4.5	2.2	
		0330	0340	17.59	16.89		-.73	.14	-.15	.70	.76	6.8	4.0	
		0402	0436	17.55	16.36		-.55	.13	-.13	1.1	.56	4.7	4.6	Fog
		0438	0512	17.97	16.28		-.44	.11	-.13	1.2	.44	3.2	4.4	Fog
		0450	0524	17.60	16.23		-.42	.11	-.15	1.4	.42	3.1	4.8	Fog
		0526	0611	17.65	16.32		-.42	.11	-.14	1.5	.43	3.1	5.0	Fog
		0613	0647	17.67	16.37		-.36	.12	-.10	1.2	.52	2.9	4.6	Fog
		0649	0724	17.67	16.32		-.52	.14	-.12	1.5	.80	4.8	6.0	Fog
		0726	0812	17.18	16.25		-.50	.12	-.14	1.3	.50	4.0	5.0	Fog
		0814	0847	17.46	16.64		-.24	.12	-.12	.8	.41	1.9	3.6	Fog
		0849	0911	17.33	17.42		-.18	.13	-.08	.3	.61	1.5	2.4	
		0924	0946	17.48	17.57		-.47	.14	-.08		.87	4.3		

BEST AVAILABLE COPY

				°C	°C	m/sec	10^{-2} °C/m	m/sec		10^{-3} °C^2/m$^{2/3}$	10^{-3} m^2/sec^3	W	watt/m^2					
	Date	Time	Time	T_s	T_{10}	U_{10}	$(\partial t/\partial z)_{10}$	U_*	R_{i10}	$C_{T,10}^2$	ε	grad	turb					
Fog 2	10/5	0514	0522	19.08	19.17	3.0	-.69	.12	-.20	2.1	.52	5.7	6.4					
		0632	0641	19.27	19.10	2.5	-.30	.087	-.16	1.6	.19	1.7	3.8					
		0730	0740	22.55	19.44	2.2	-.48	.13	-.12	1.7	.57	4.1	5.8					
		0829	0903	18.35	17.90	1.3	-.82	.13	-.22	.9	.67	7.4	4.4	Fog				
		0905	0939	18.37	18.10	.7	0.23	.10	-.10	.6	.30	1.5	2.8	Fog				
		0952	1027	19.25	18.13	1.6		.09		1.2	.24		3.6					
		1200	1222	21.75	20.24	3.4	-1.79	.09	-.74	1.9	.20	13.8	4.4					
Fog 3	10/8	0848	0854		21.02	3.1		.14		1.8	.76		6.4					
		0945	0956		19.27	3.4		.24		2.5	4.1		12.8					
		1200	1241		16.10	4.3	-1.15	.18	-.24	1.1	.97	14.9	5.4	Fog				
		1241	1317		17.03	3.4	.12	.12	.09	.5	.45	- .3	-1.0					
		1416	1452		18.36	3.0	2.94	.17	.42	.25	1.6	0	0					
		1452	1532		17.96	3.0	2.63	.20	.35	.50		0	0					
		1532	1605		16.33	3.0	-2.49	.14	-.56	.30		24.7	3.0	Fog				
		1605	1642		16.05	3.0	-1.02	.17	-.14	.10		10.5	1.6	Fog				
		1642	1718		15.96	3.0	1.10	.16	.14	.12		- 2.3	- .6	Fog				
		1719	1753		16.33	3.1	4.10	.15	1.00	1.10	.90	0	0	Fog				
		1753	1805		17.24	3.3	2.44	.096	1.09	1.5	.25	0	0					
		2000	2017		17.54	4.1	1.09	.18	.14	.06	1.6	- 2.6	- .6					

BEST AVAILABLE COPY

				°C	m/sec		10^{-2}°c/m	m/sec		10^{-3}°c²/m$^{2/3}$	10^{-3}m²/sec³		W	watt/m²	
	Date	Time	Time	T_s	T_{10}	U_{10}	$(\partial t/\partial z)_{10}$	U_*	R_{i10}	C^2_{T10}	ϵ_{10}	grad	turb		
Fog 4	10/9	0747	0811		16.84	8.3	- .34	.41	-.01	1.5	19	7.9	17.4		
		0811	0835		15.62	8.2	-1.31	.41	-.03	1.5	20	30.7	17.0		
		0835	0859		15.45	8.1	-1.83	.43	-.04	.9	23	46.2	15.4	Fog	
		0913	0951		15.25	7.8	-1.83	.40	-.05	1.4	18	43.0	15.8	Fog	
		1200	1220		15.36	6.8	- .96	.37	-.03	2.3	15	20.9	19.8		
		1320	1341		15.40	6.7	.24	.37	.01	1.0	14	-4.6	-13		

BEST AVAILABLE COPY

Figure 1.

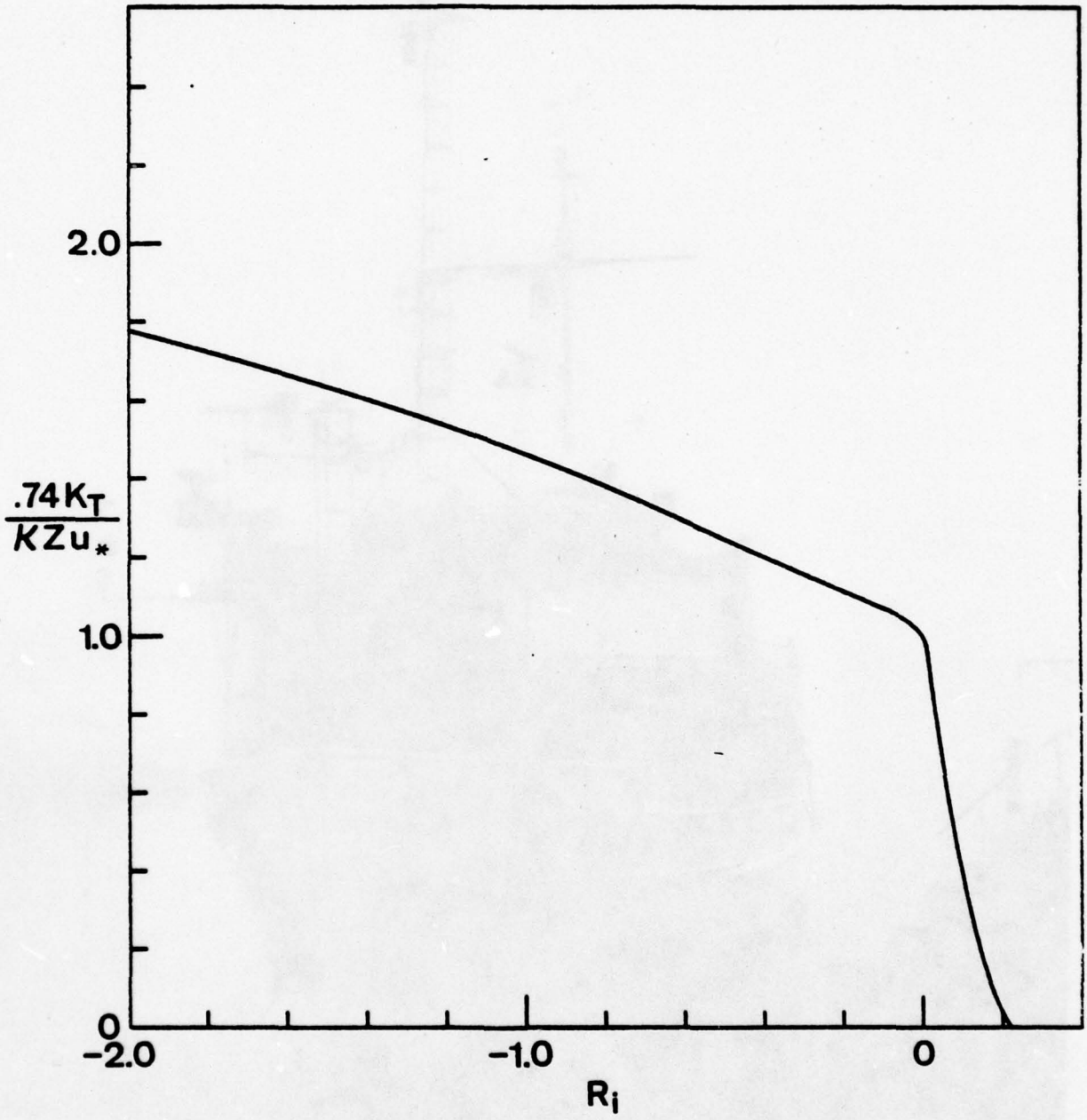

Figure 2.

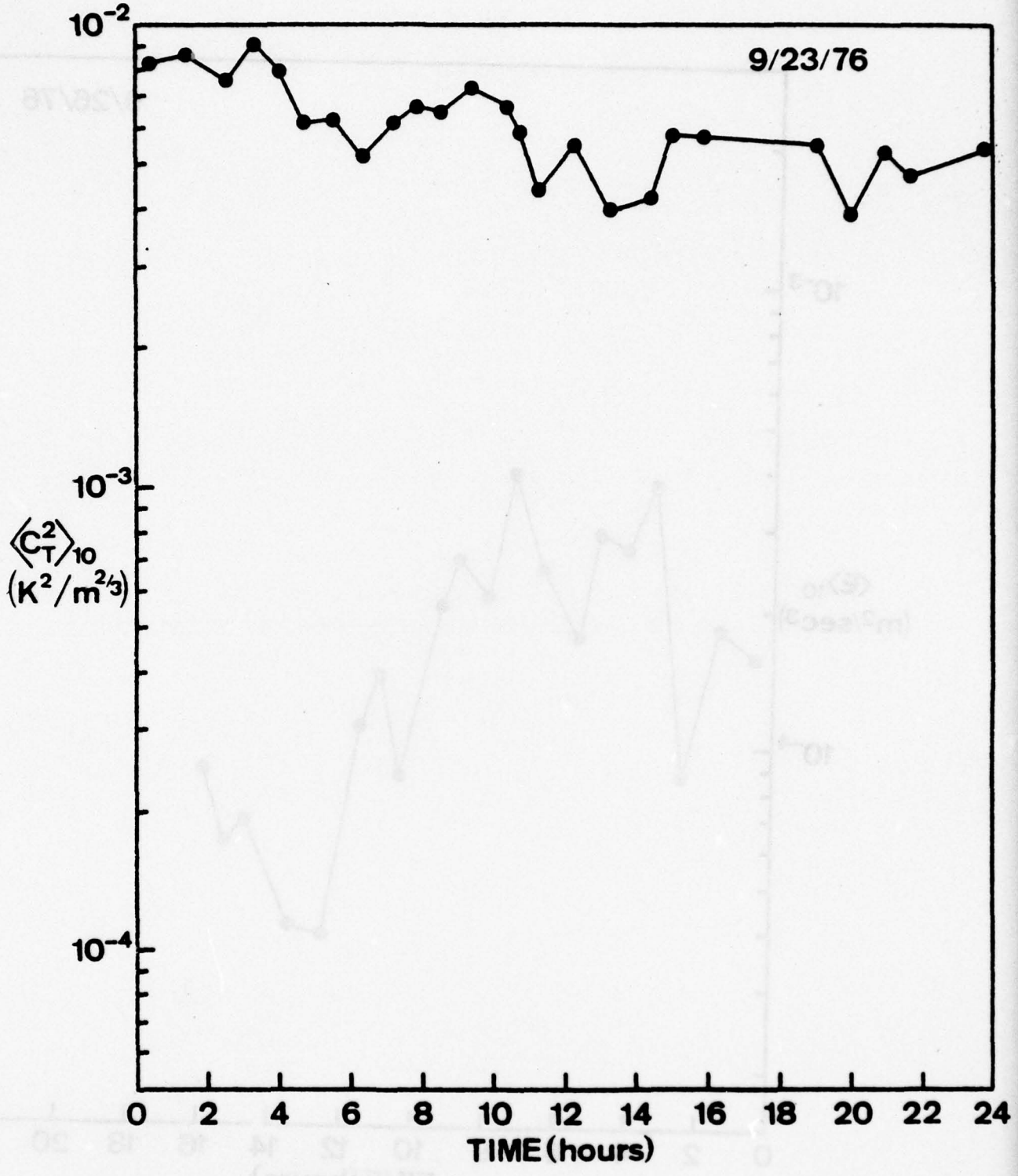
9/23/76
10^{-2}
10^{-3}
10^{-4}
$\langle C_T^2 \rangle_{10}$
$(K^2/m^{2/3})$
0 2 4 6 8 10 12 14 16 18 20 22 24
TIME (hours)

Figure 3a.

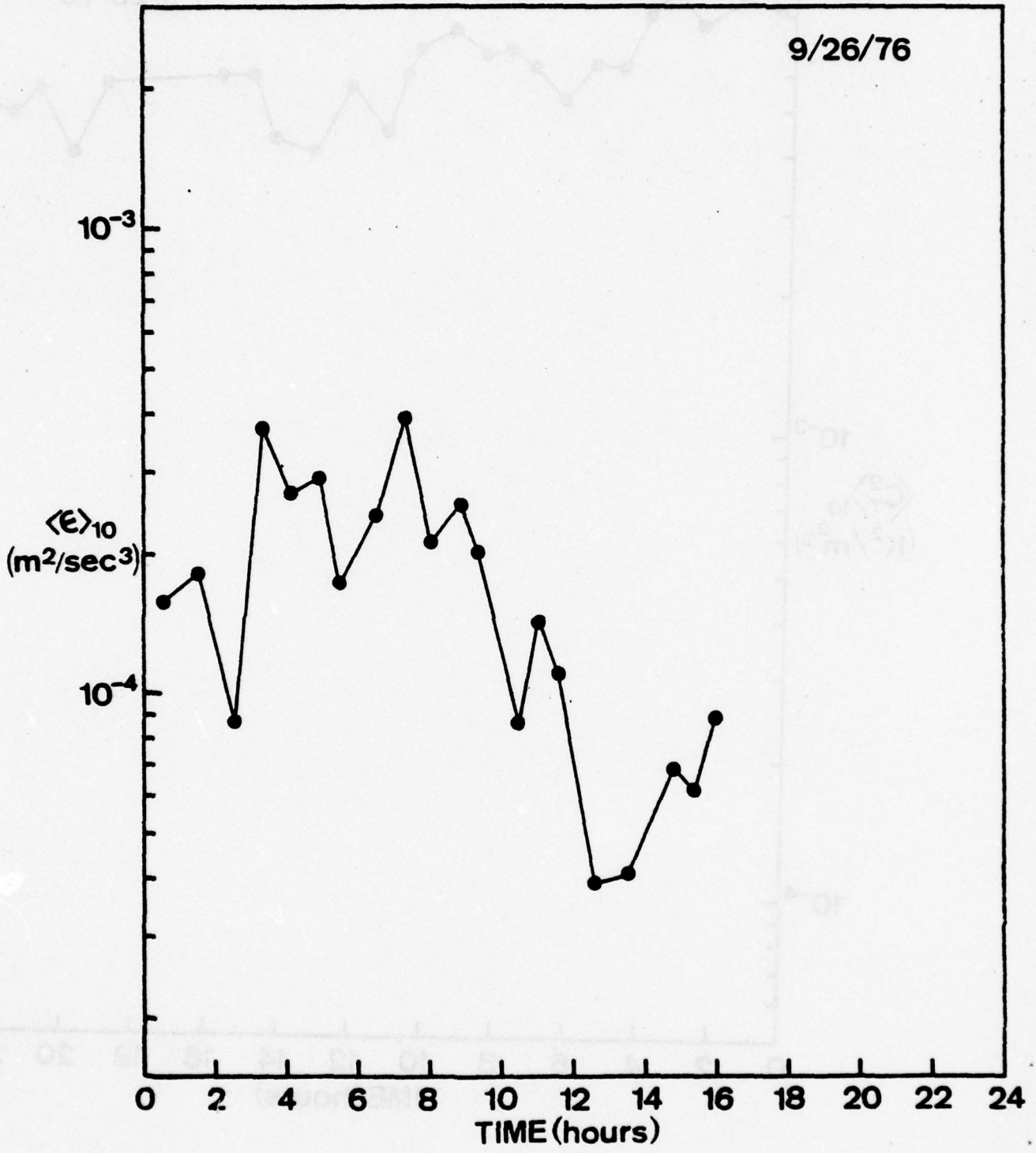
9/26/76
10^{-3}
$\langle\epsilon\rangle_{10}$
(m^2/sec^3)
10^{-4}
0
2
4
6
8
10
12
14
16
18
20
22
24
TIME (hours)

Figure 3b.

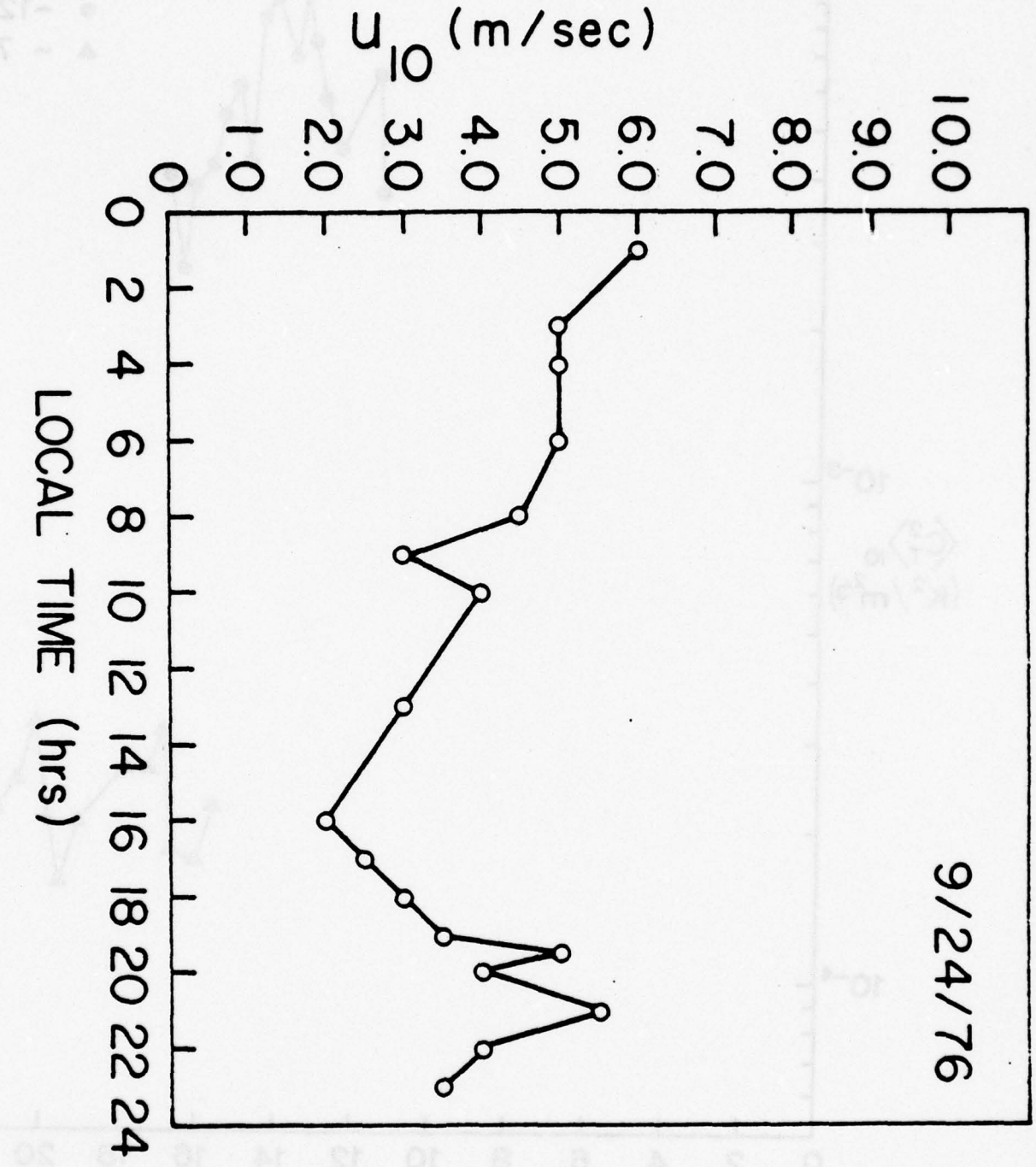
U_{10} (m/sec)
0
1.0
2.0
3.0
4.0
5.0
6.0
7.0
8.0
9.0
10.0
0 2 4 6 8 10 12 14 16 18 20 22 24
LOCAL TIME (hrs)
9/24/76

Figure 3c.

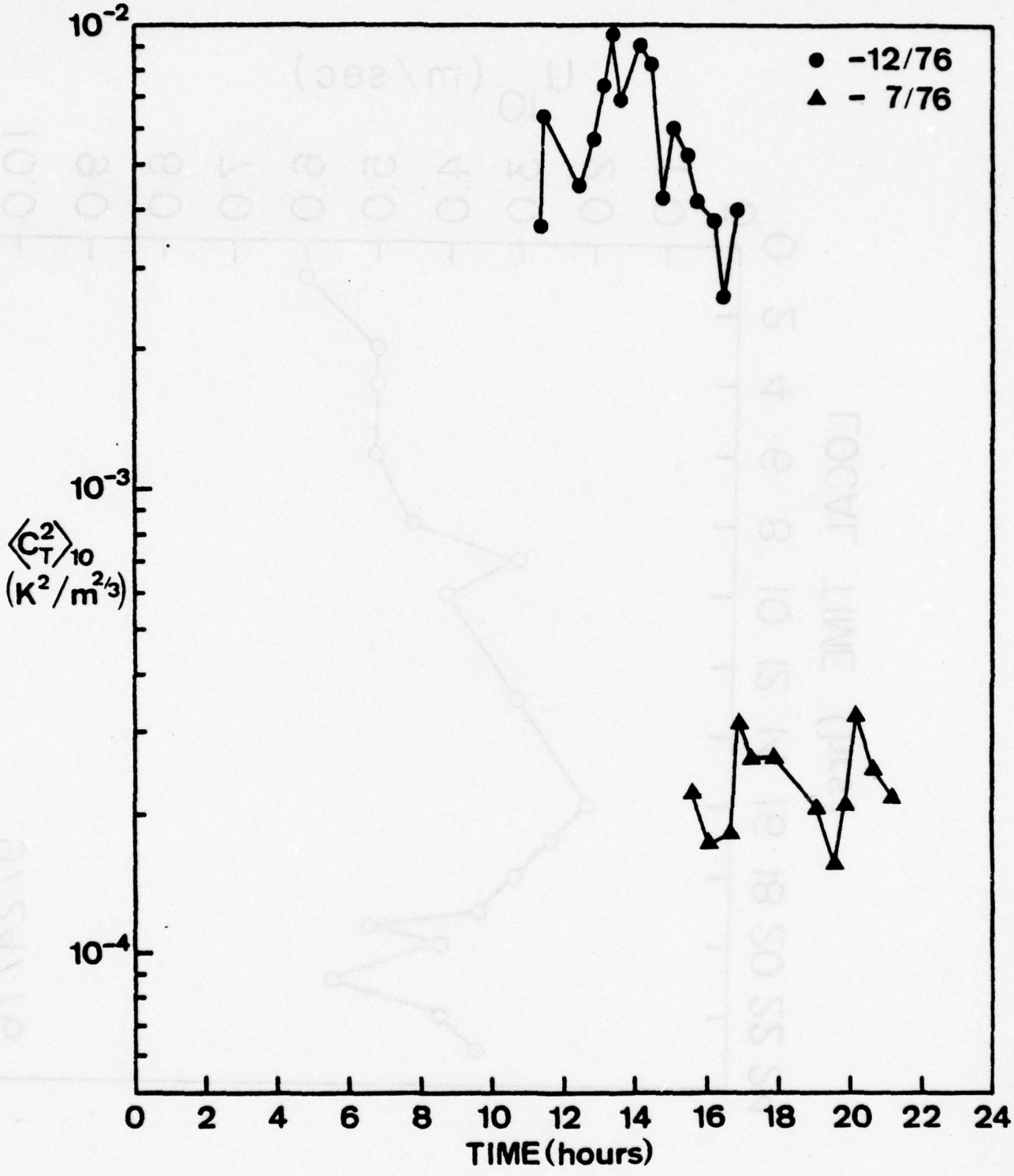
10^-2
10^-3
10^-4
● -12/76
▲ - 7/76
⟨C_T^2⟩_10
(K^2/m^2/3)
0 2 4 6 8 10 12 14 16 18 20 22 24
TIME (hours)

Figure 4.

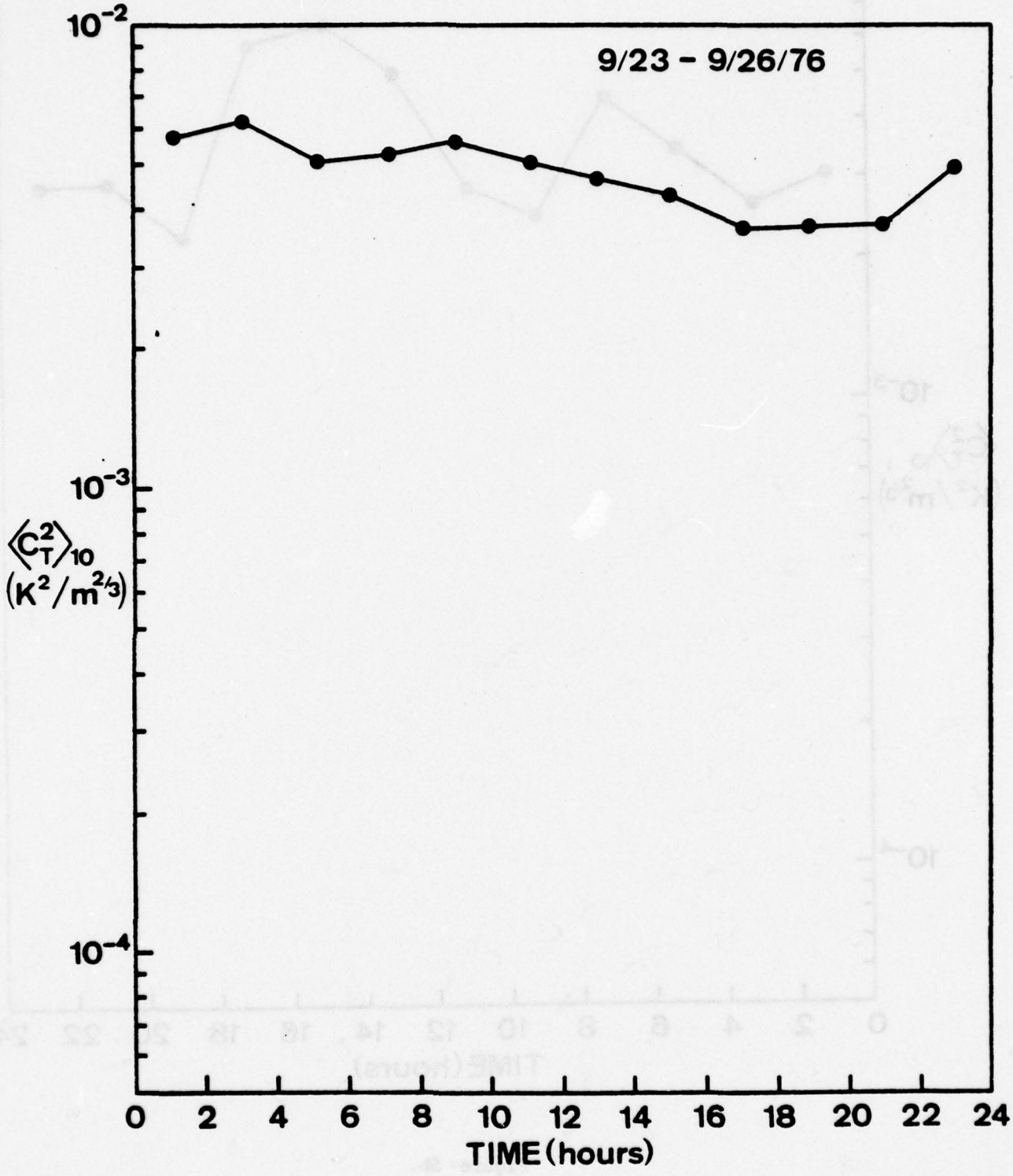
9/23 - 9/26/76
10^{-2}
10^{-3}
10^{-4}
$\langle C_T^2 \rangle_{10}$
$(K^2/m^{2/3})$
0 2 4 6 8 10 12 14 16 18 20 22 24
TIME (hours)

Figure 5a.

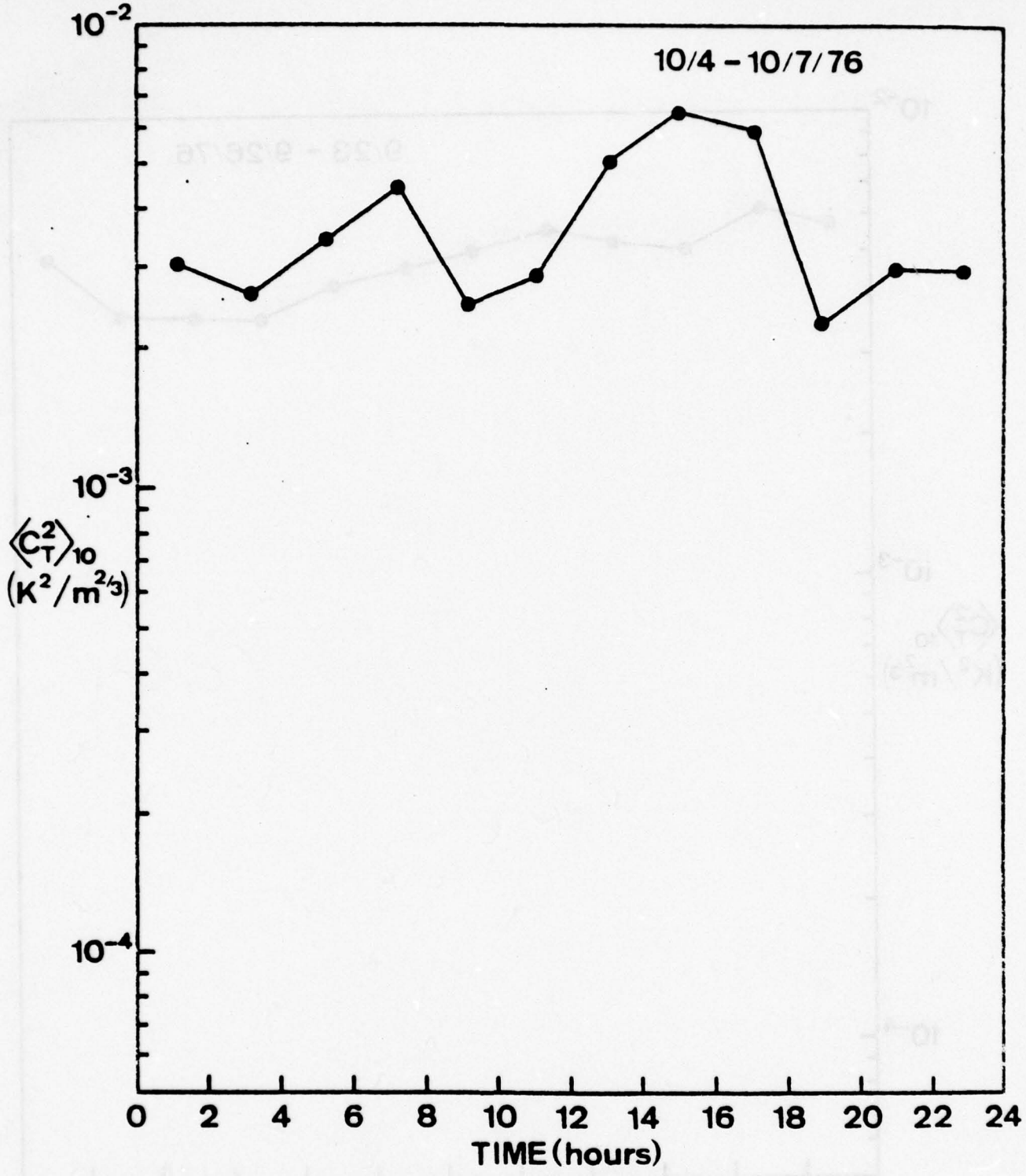
10/4 - 10/7/76
10^{-2}
10^{-3}
10^{-4}
$\langle C_T^2 \rangle_{10}$
$(K^2/m^{2/3})$
0 2 4 6 8 10 12 14 16 18 20 22 24
TIME (hours)

Figure 5b.

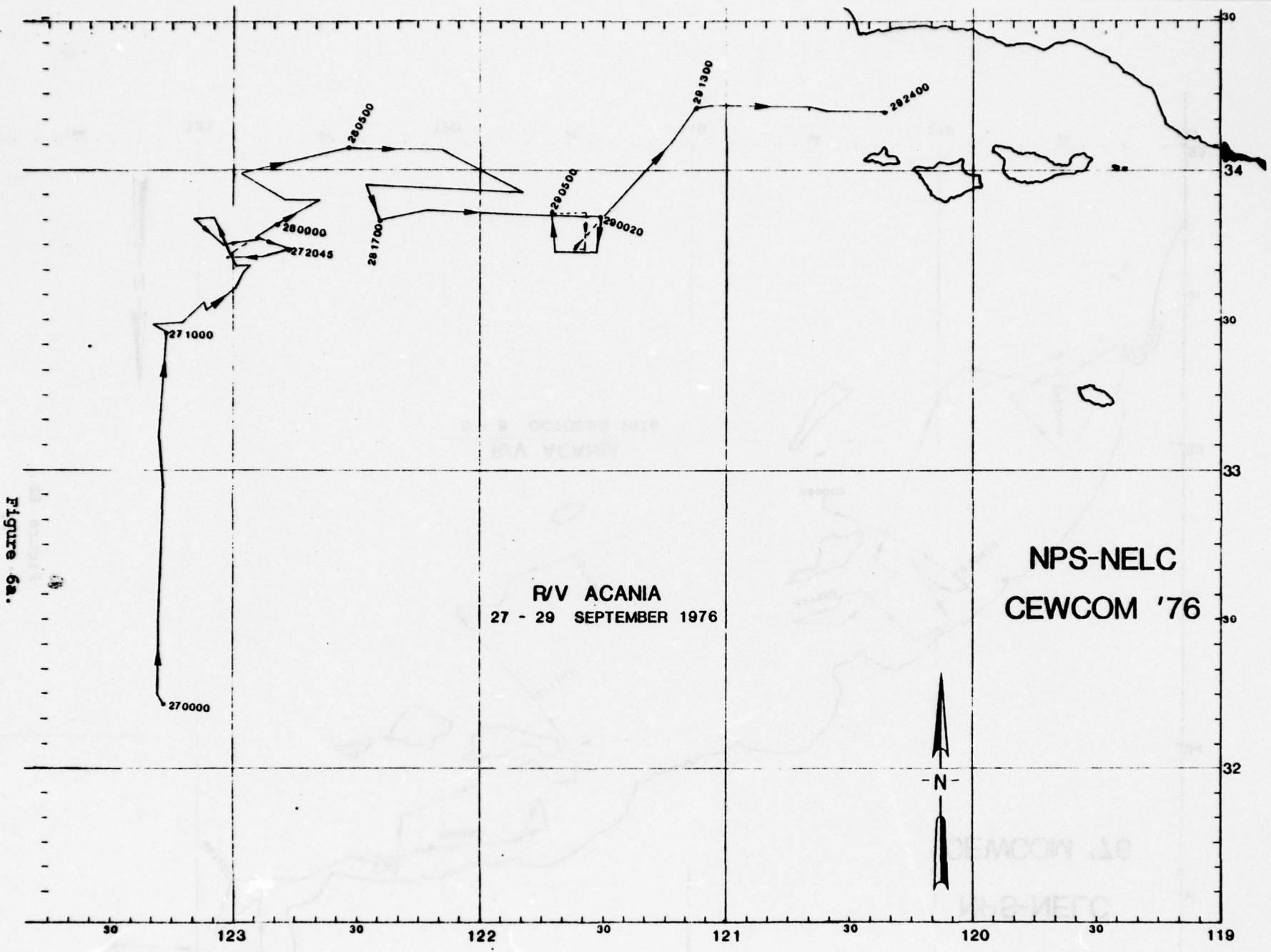
280500
291300
292400
290500
290020
280000
272045
281700
271000
270000
R/V ACANIA
27 - 29 SEPTEMBER 1976
NPS-NELC
CEWCOM '76
N
34
33
32
123
122
121
120
119

Figure 6a.

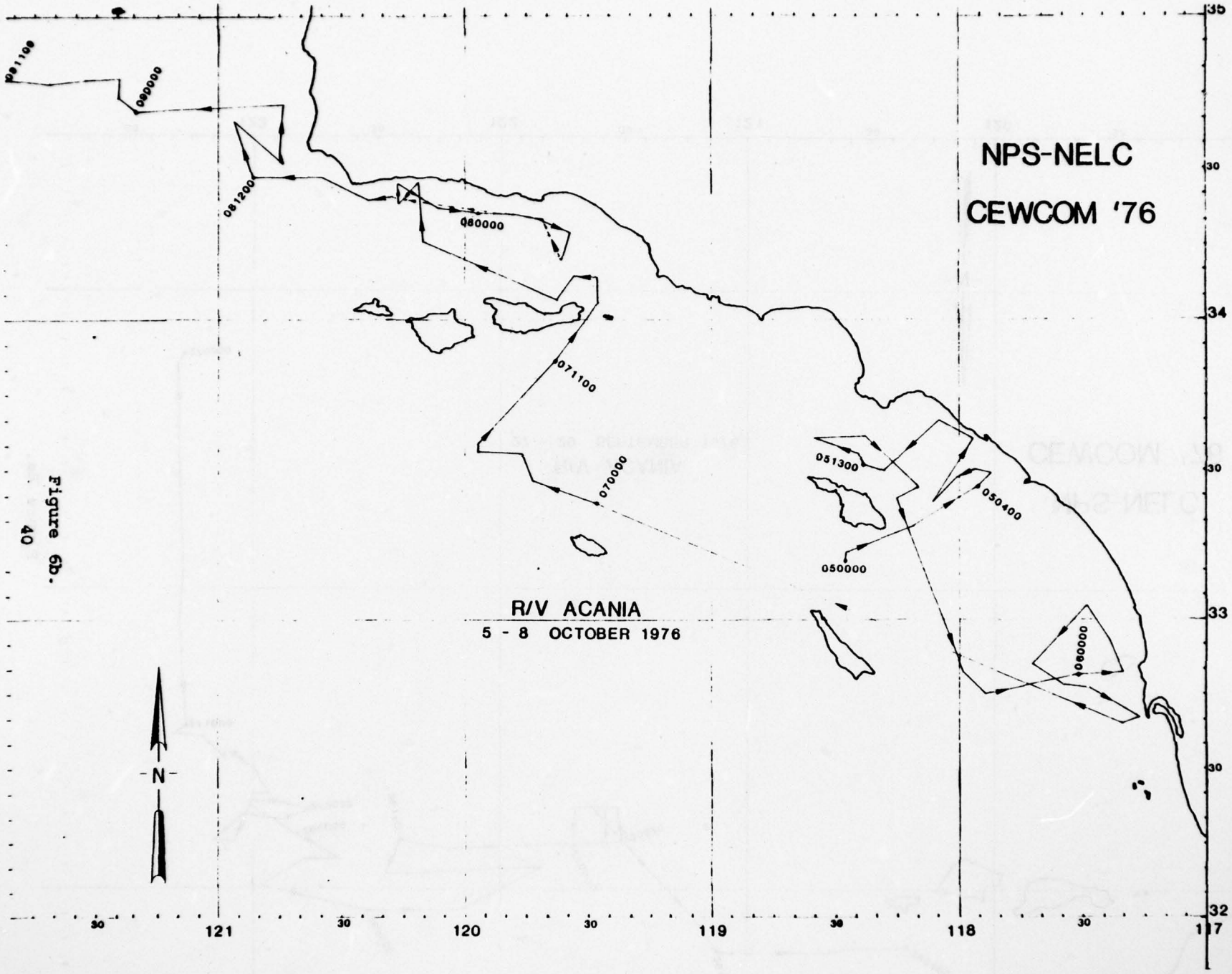
NPS-NELC
CEWCOM '76
R/V ACANIA
5 - 8 OCTOBER 1976
081100
080000
081200
080000
071100
070000
051300
050400
050000
060000
N
35
30
34
30
33
30
32
30
121
30
120
30
119
30
118
30
117

Figure 6b.

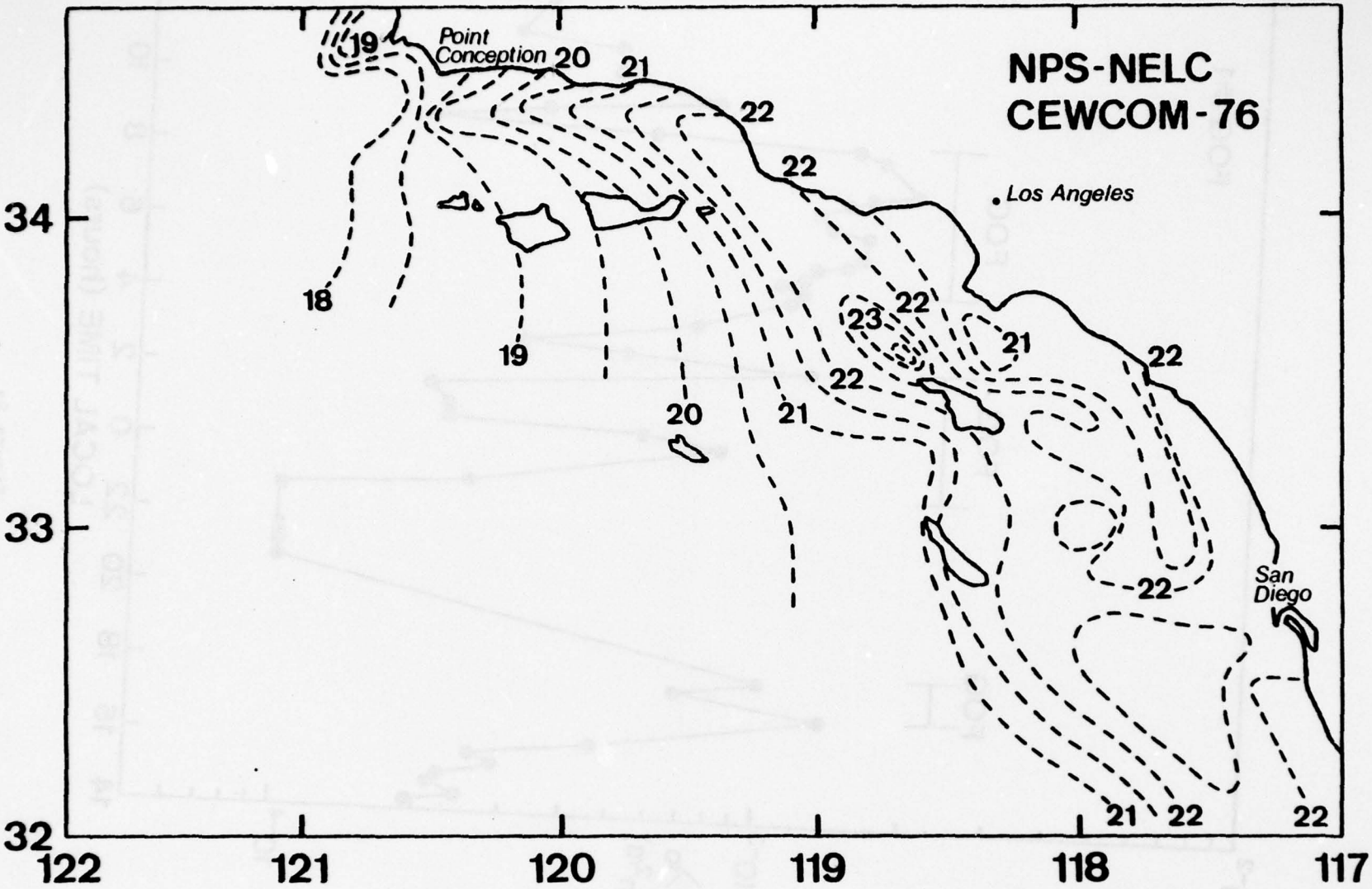
NPS-NELC
CEWCOM-76
Point
Conception
Los Angeles
San
Diego
34
33
32
122
121
120
119
118
117

Figure 7.

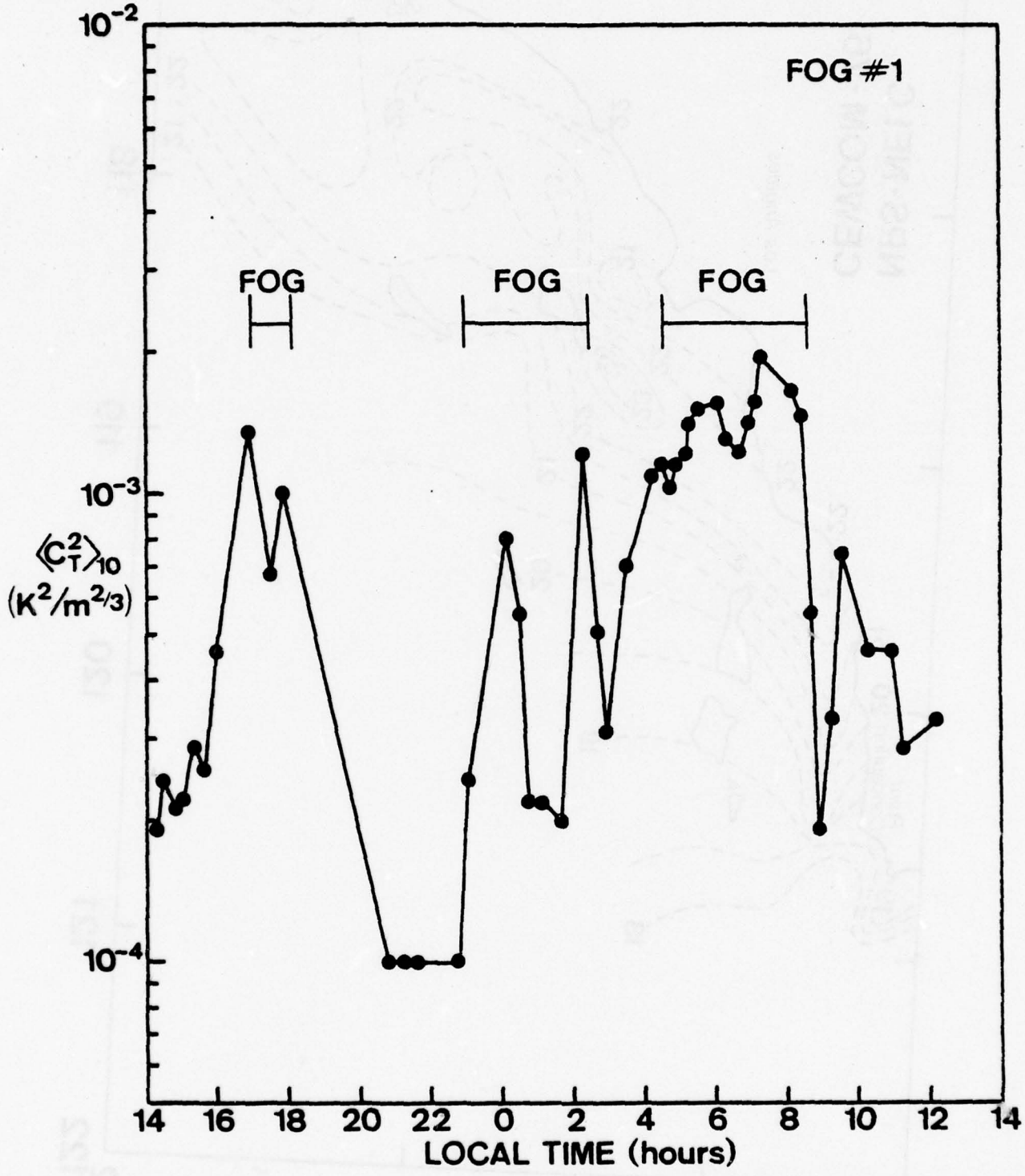
FOG #1
FOG
FOG
FOG
10^{-2}
10^{-3}
10^{-4}
$\langle C_T^2 \rangle_{10}$
$(K^2/m^{2/3})$
14 16 18 20 22 0 2 4 6 8 10 12 14
LOCAL TIME (hours)

Figure 8a.

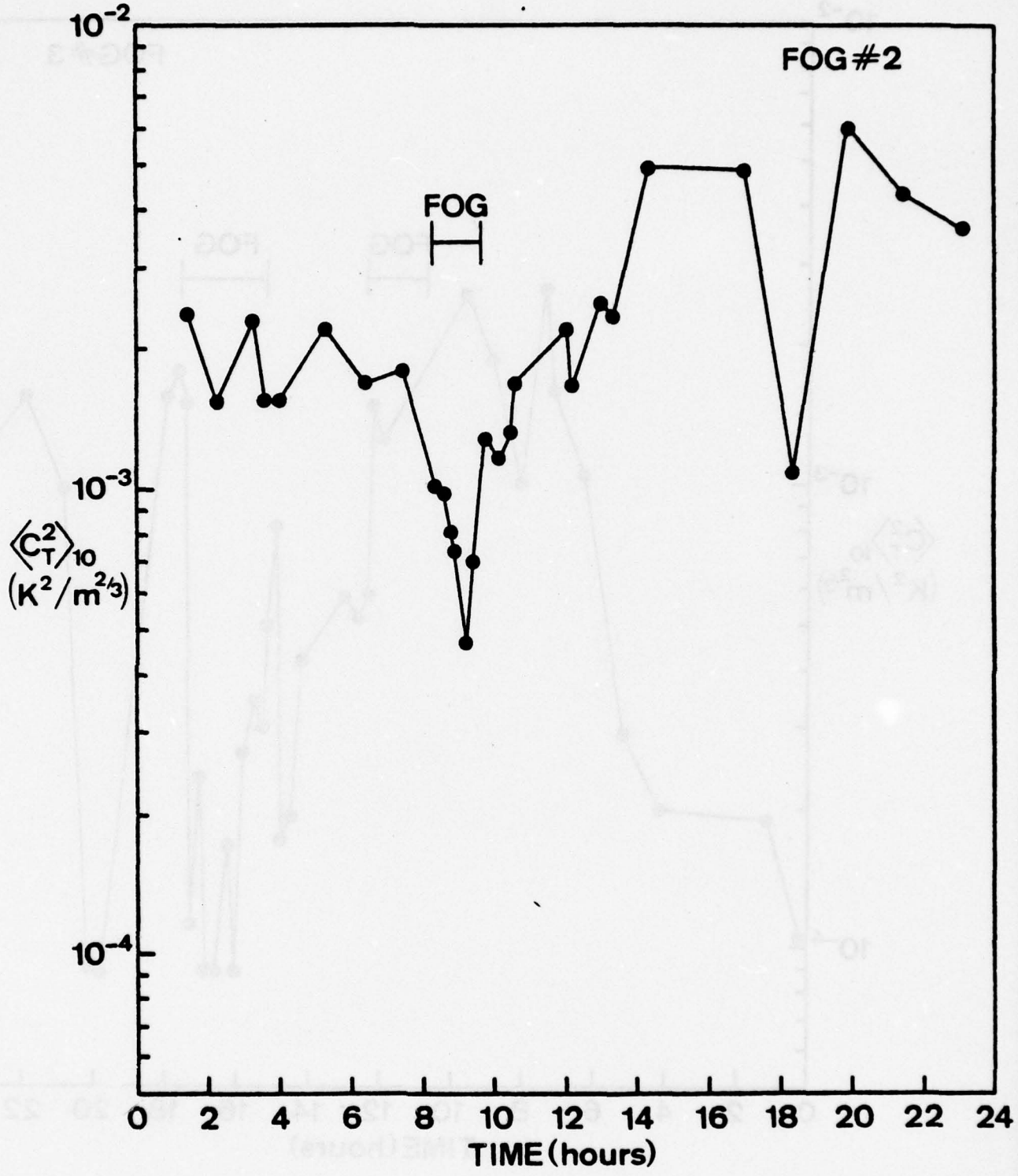
FOG#2
FOG
10^{-2}
10^{-3}
10^{-4}
$\langle C_T^2 \rangle_{10}$
$(K^2/m^{2/3})$
0 2 4 6 8 10 12 14 16 18 20 22 24
TIME (hours)

Figure 8b.

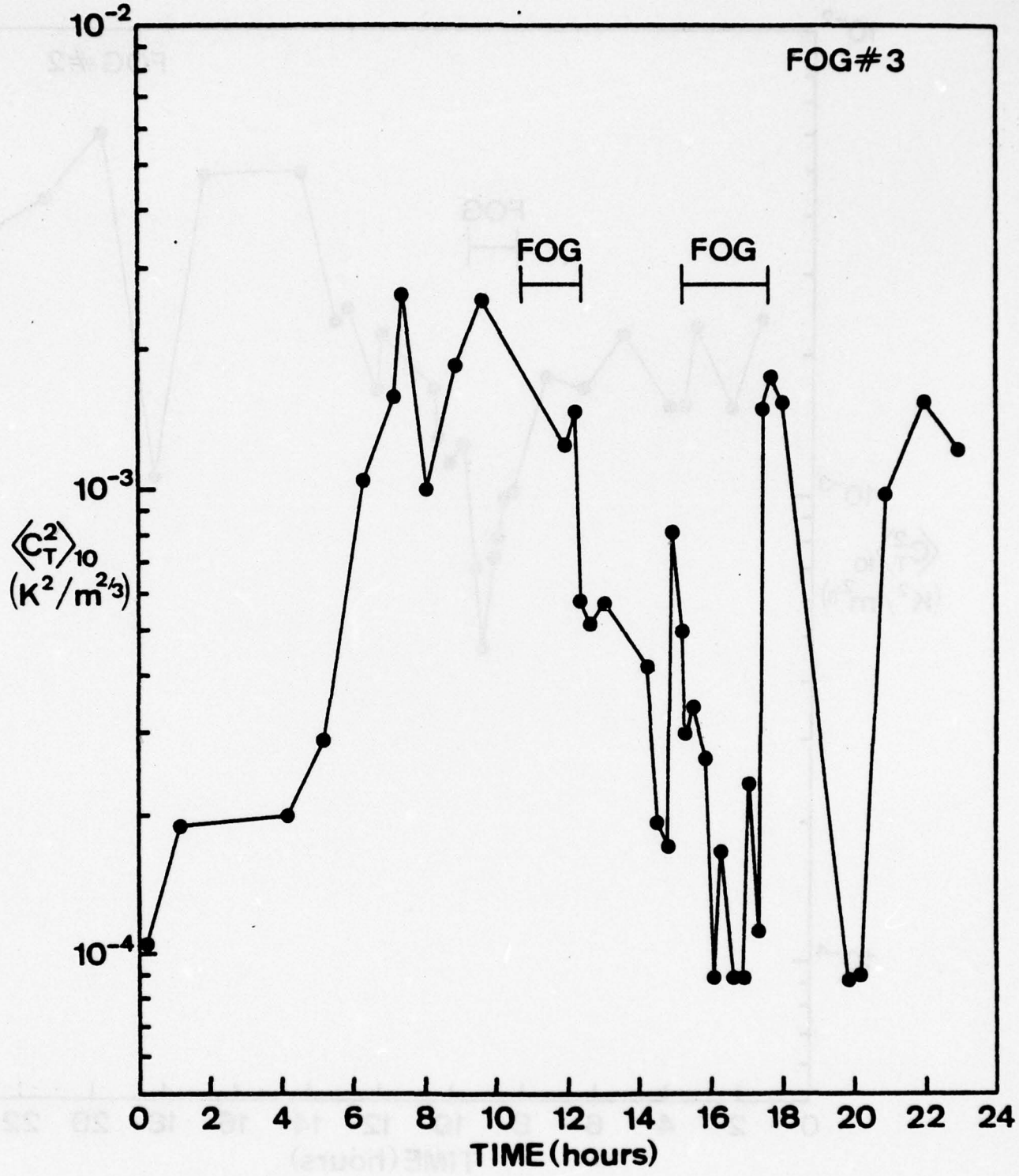
FOG#3
FOG
FOG
10^{-2}
10^{-3}
10^{-4}
$\langle C_T^2 \rangle_{10}$
$(K^2/m^{2/3})$
0 2 4 6 8 10 12 14 16 18 20 22 24
TIME (hours)

Figure 8c.

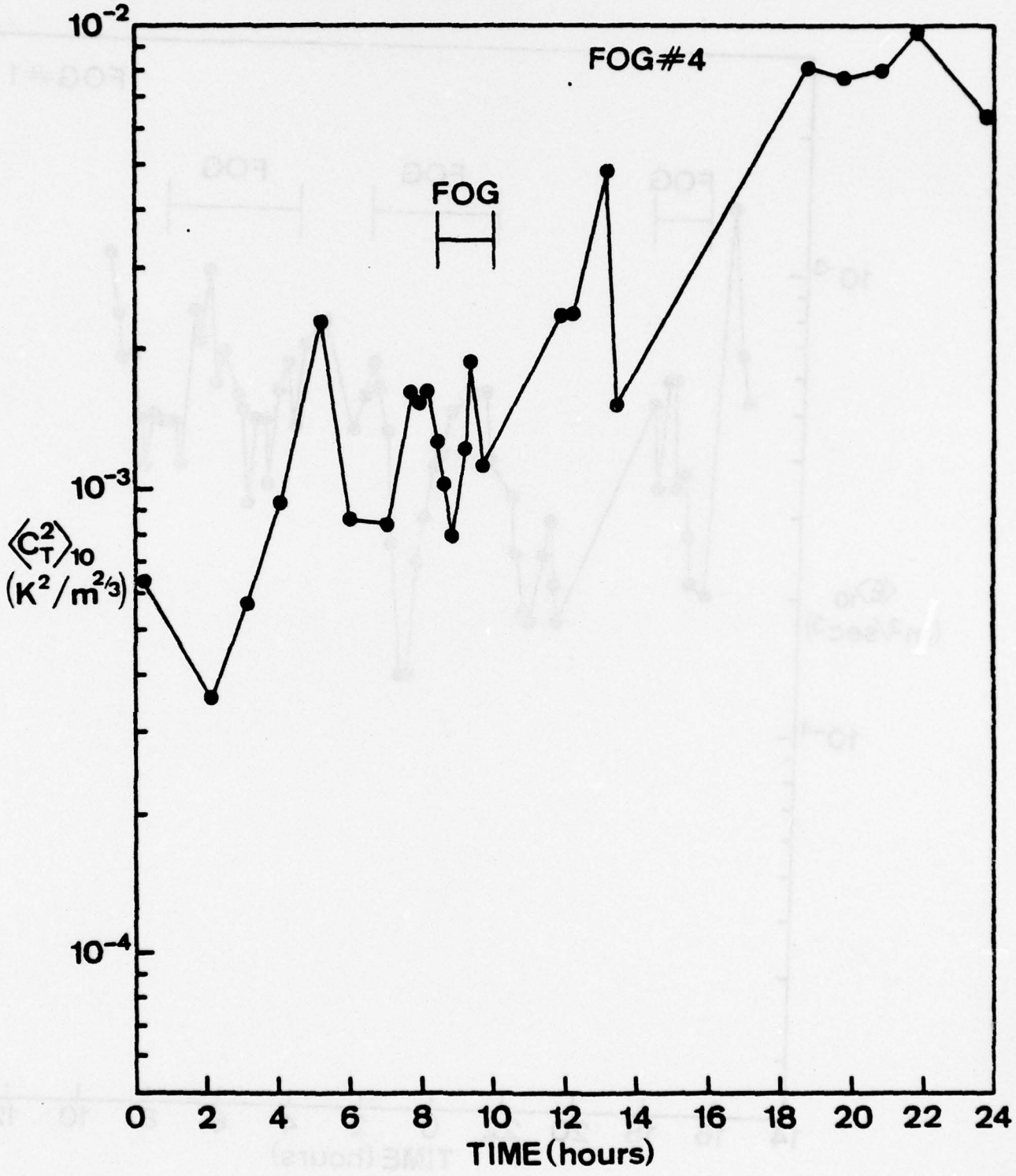
FOG#4
FOG
10^{-2}
10^{-3}
10^{-4}
$\langle C_T^2 \rangle_{10}$
$(K^2/m^{2/3})$
0 2 4 6 8 10 12 14 16 18 20 22 24
TIME (hours)

Figure 8d.

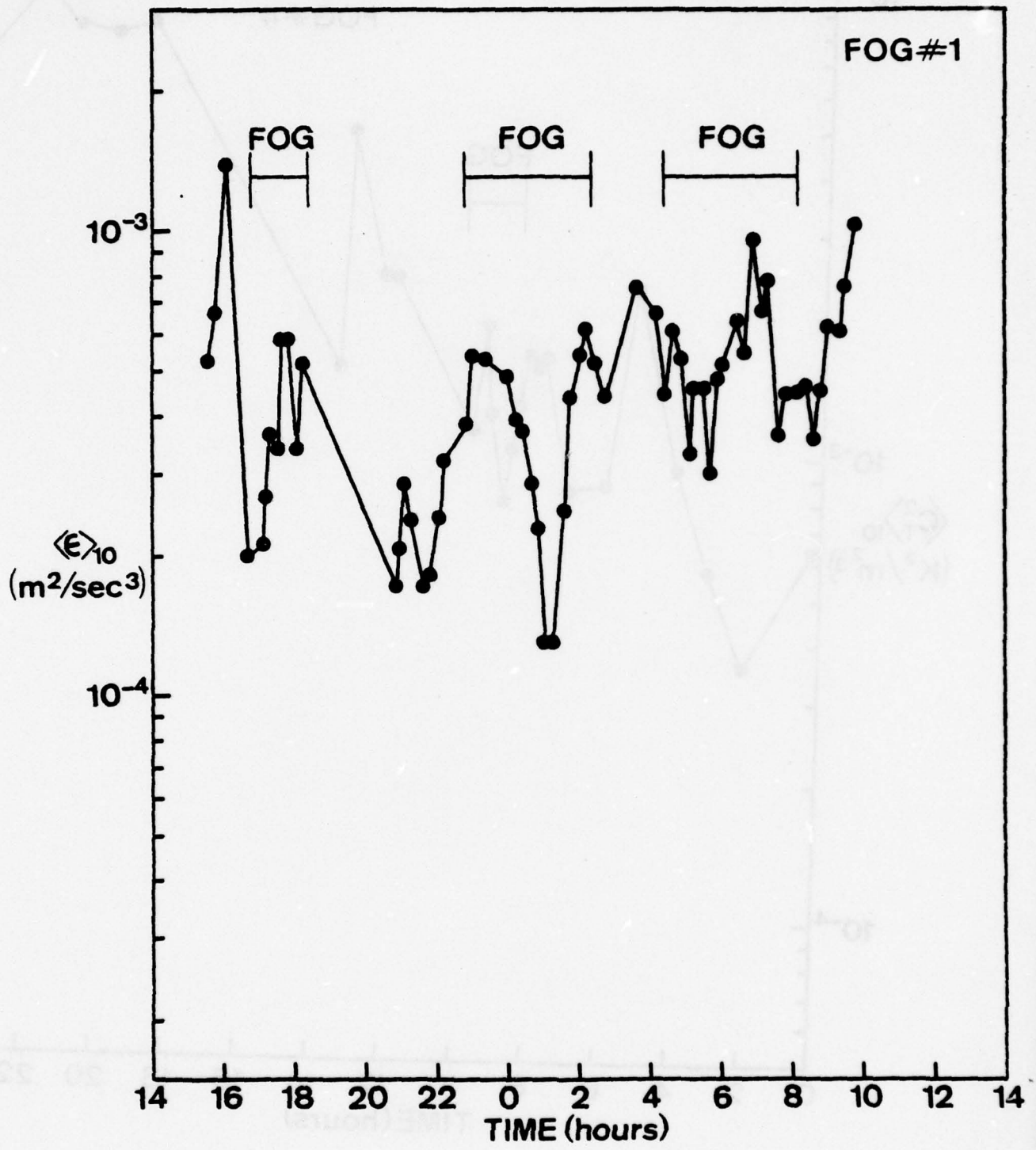
FOG#1
FOG
FOG
FOG
10^{-3}
10^{-4}
$\langle\epsilon\rangle_{10}$
(m^2/sec^3)
14
16
18
20
22
0
2
4
6
8
10
12
14
TIME (hours)

Figure 9a.

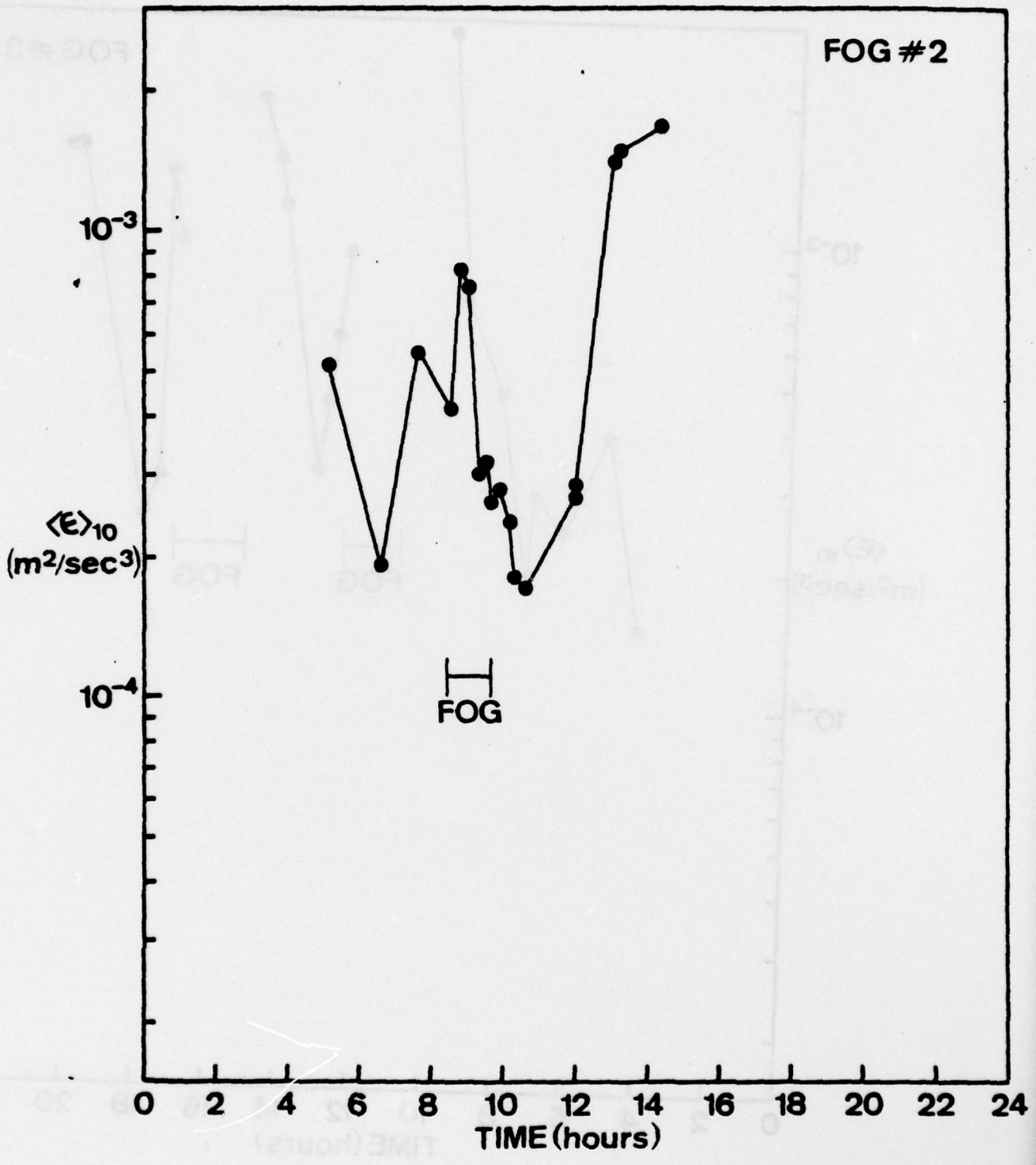
FOG #2
10^{-3}
$\langle E \rangle_{10}$
(m^2/sec^3)
10^{-4}
FOG
0
2
4
6
8
10
12
14
16
18
20
22
24
TIME (hours)

Figure 9b.

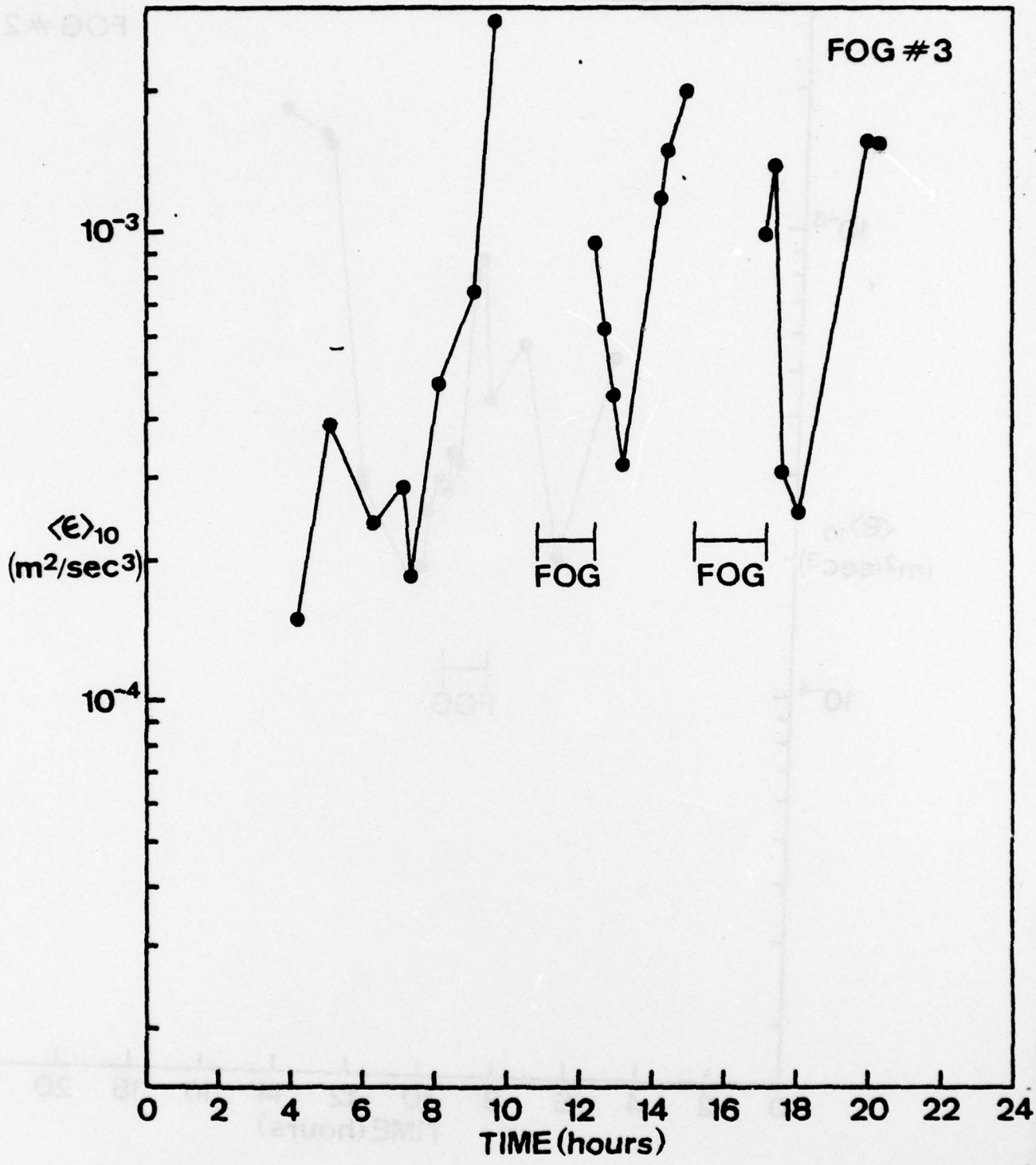
FOG #3
10^{-3}
$\langle\epsilon\rangle_{10}$
(m^2/sec^3)
10^{-4}
FOG
FOG
0 2 4 6 8 10 12 14 16 18 20 22 24
TIME (hours)

Figure 9c.

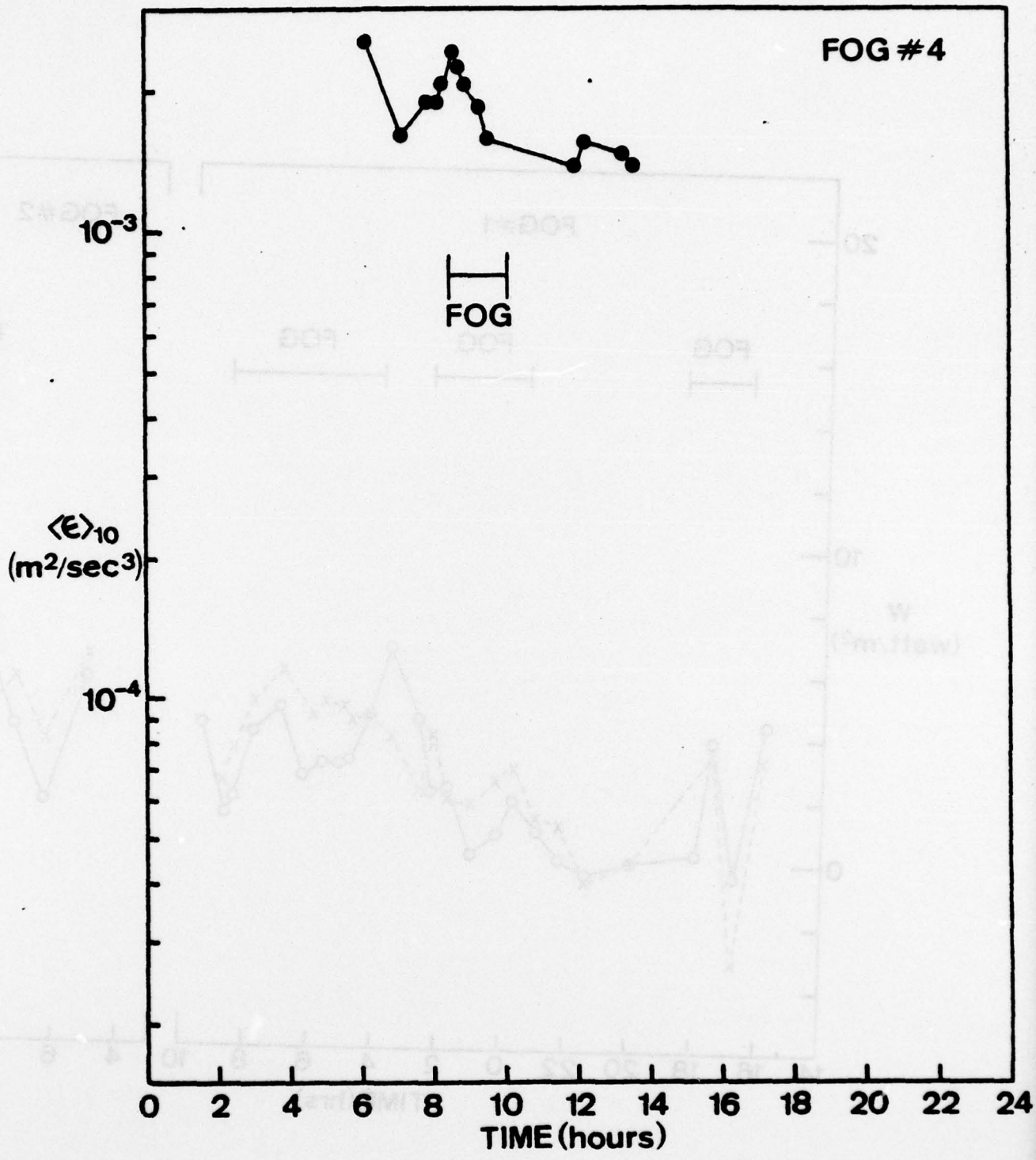
FOG #4
FOG
10^{-3}
$\langle\epsilon\rangle_{10}$
(m^2/sec^3)
10^{-4}
0 2 4 6 8 10 12 14 16 18 20 22 24
TIME (hours)

Figure 9d.

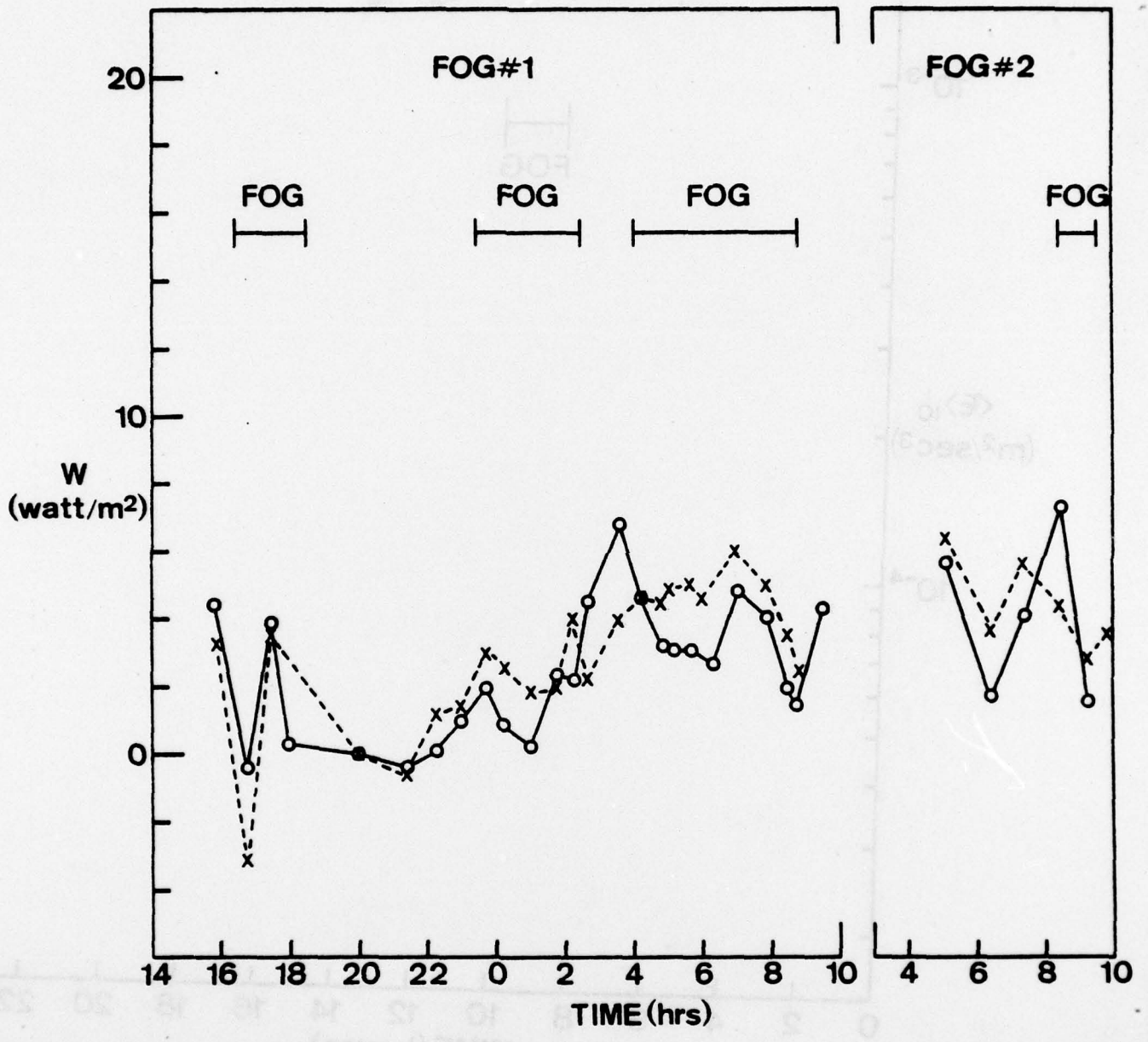
FOG#1
FOG#2
FOG
FOG
FOG
FOG
20
10
0
W
(watt/m²)
14
16
18
20
22
0
2
4
6
8
10
4
6
8
10
TIME (hrs)

Figure 10a.

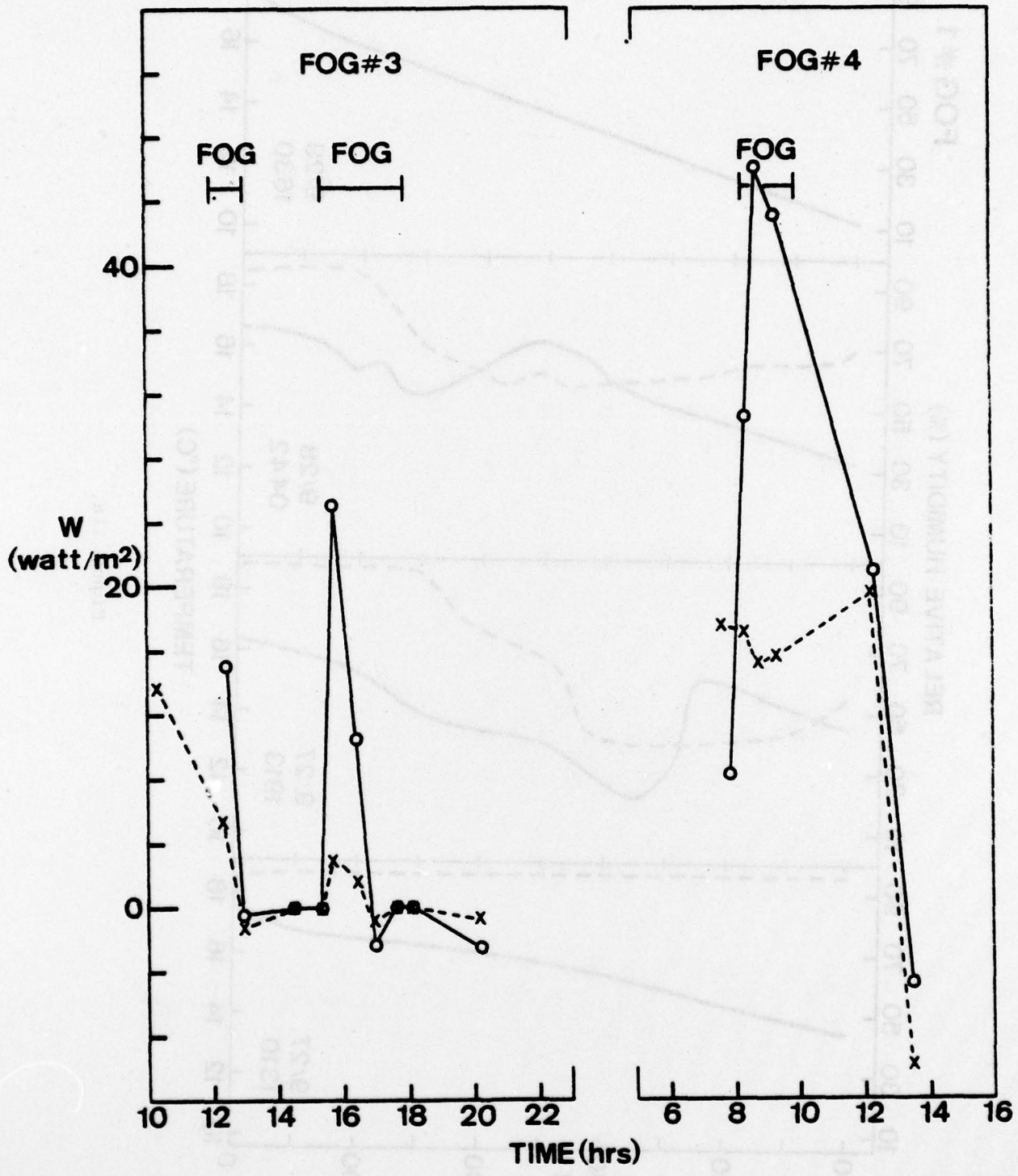
FOG#3
FOG#4
FOG
FOG
FOG
40
W
(watt/m2)
20
0
10
12
14
16
18
20
22
6
8
10
12
14
16
TIME(hrs)

Figure 10b.

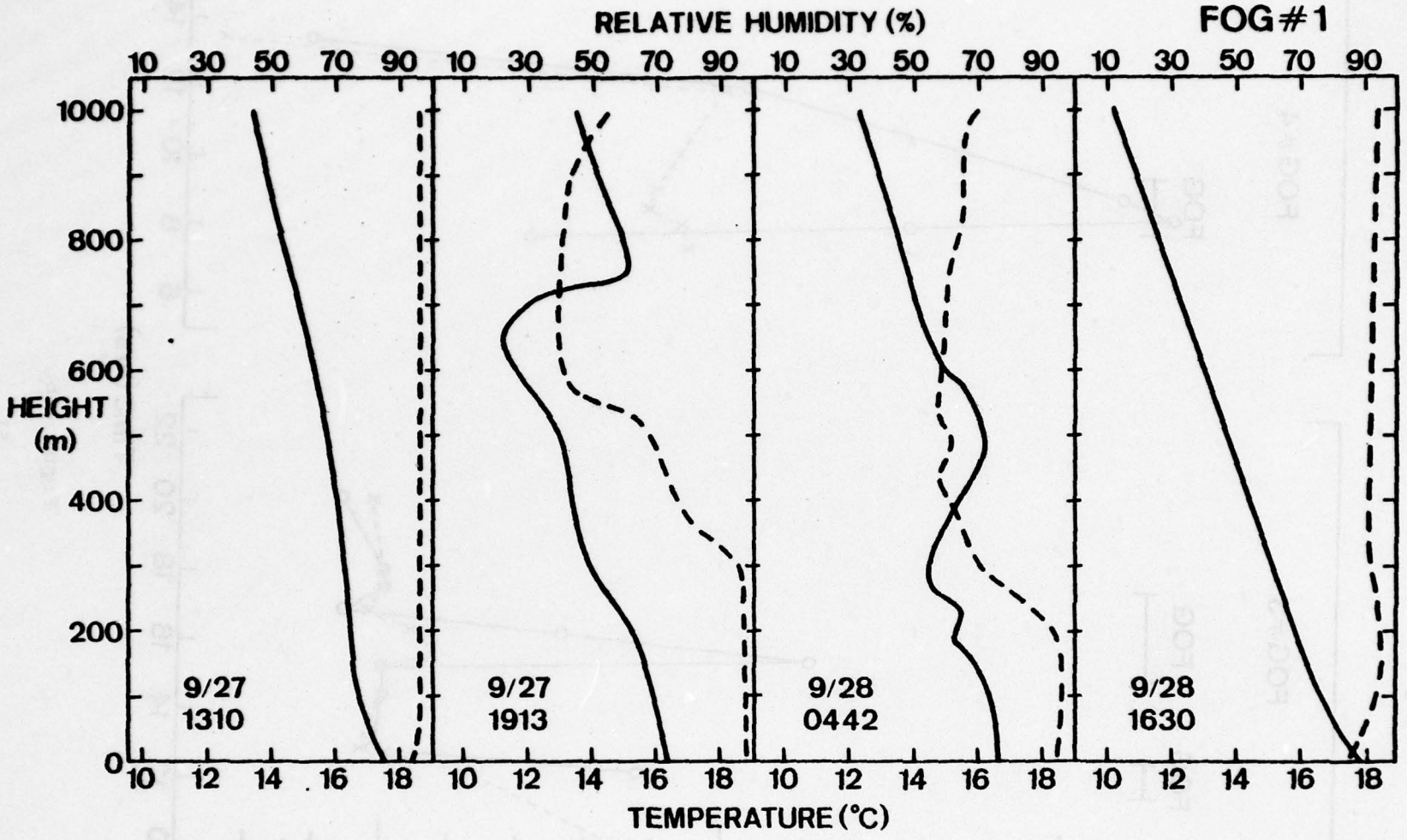
RELATIVE HUMIDITY (%)
FOG#1
10 30 50 70 90
1000
800
600
400
200
0
HEIGHT (m)
9/27 1310
9/27 1913
9/28 0442
9/28 1630
10 12 14 16 18
TEMPERATURE (°C)

Figure 11a.

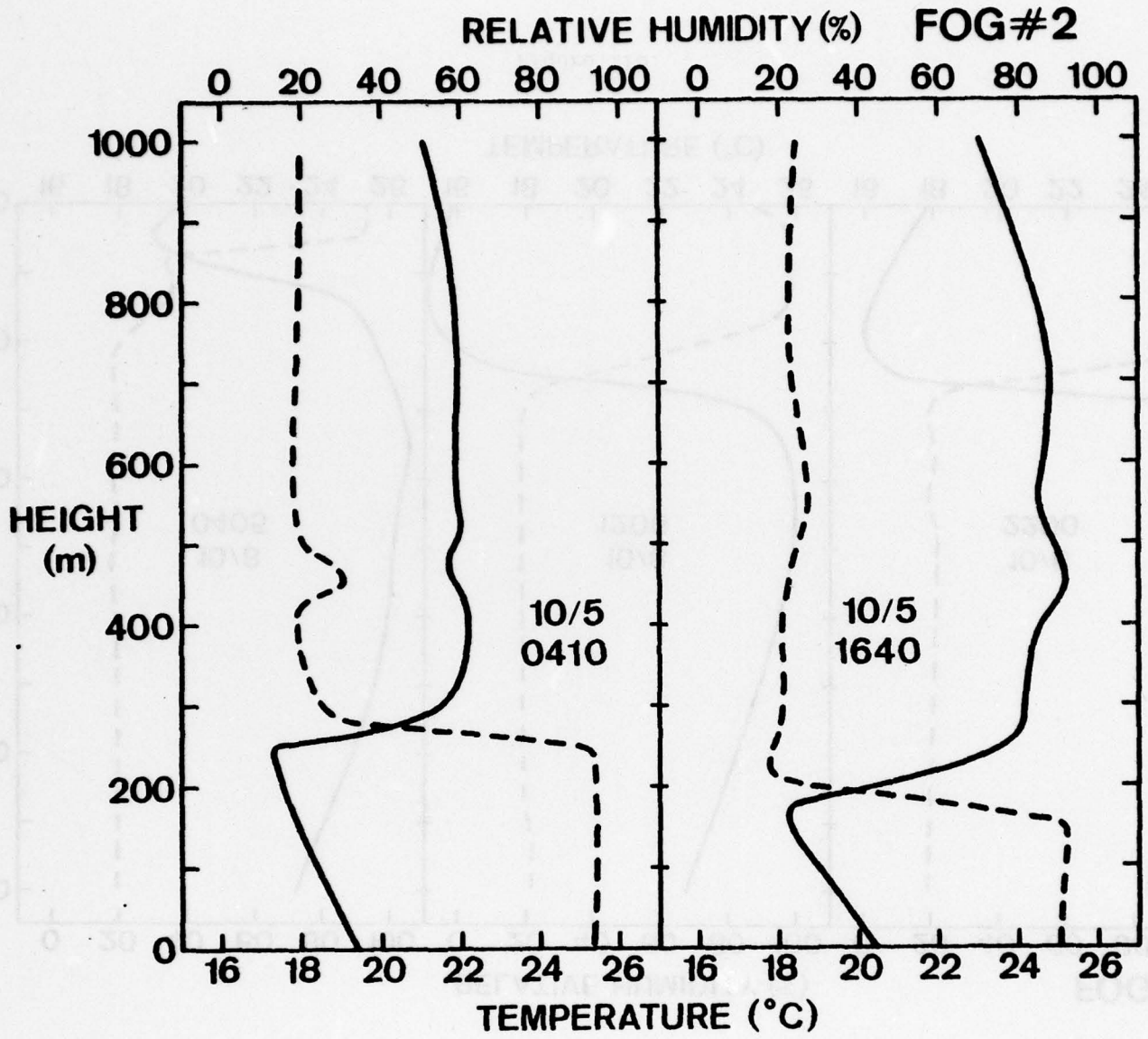
RELATIVE HUMIDITY (%)
FOG#2
0 20 40 60 80 100
0 20 40 60 80 100
1000
800
600
HEIGHT
(m)
400
200
0
10/5
0410
10/5
1640
16 18 20 22 24 26
16 18 20 22 24 26
TEMPERATURE (°C)

Figure 11b.

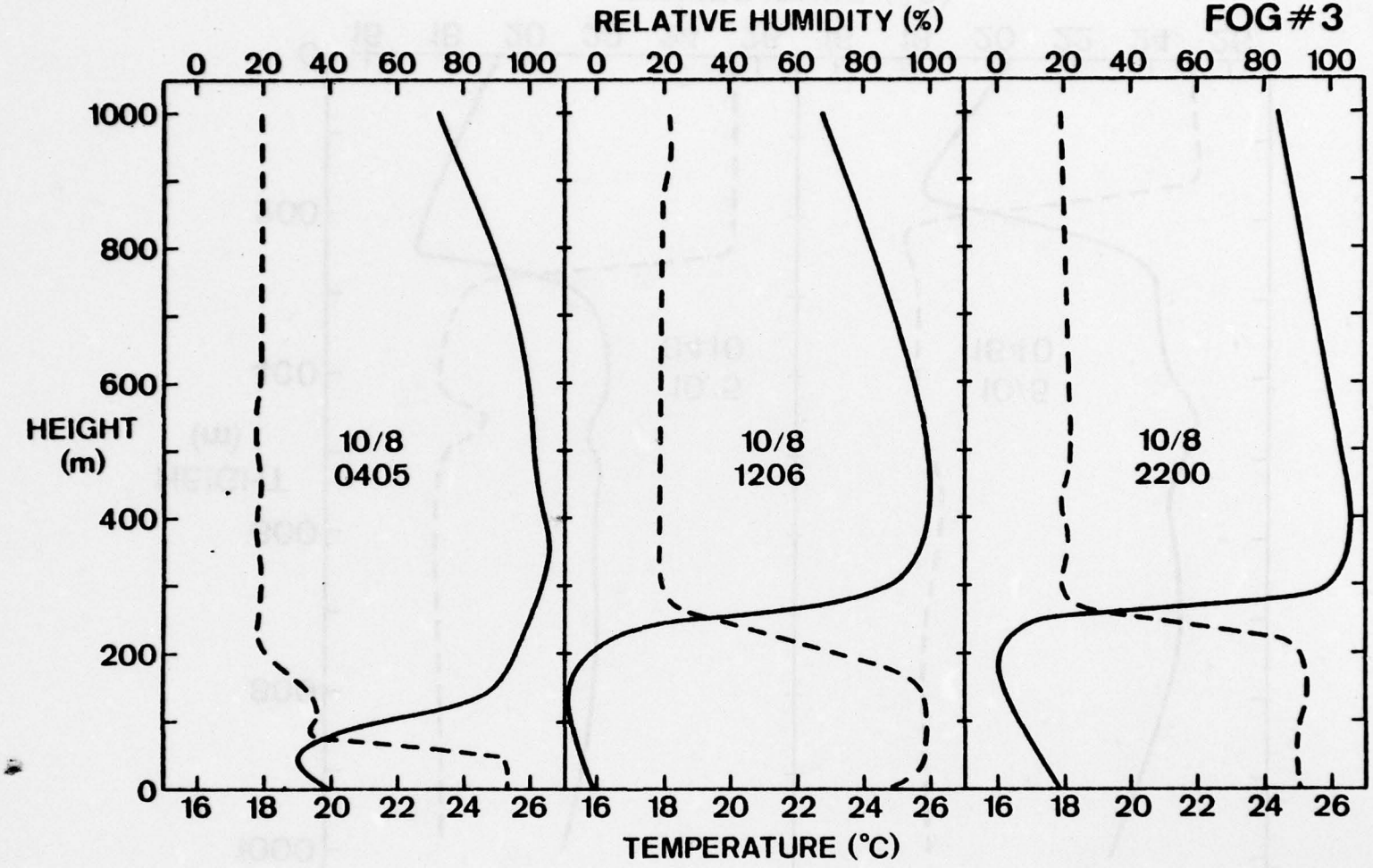
RELATIVE HUMIDITY (%)
FOG#3
0 20 40 60 80 100
1000
800
600
400
200
0
HEIGHT (m)
10/8 0405
10/8 1206
10/8 2200
16 18 20 22 24 26
TEMPERATURE (°C)

Figure 11c.

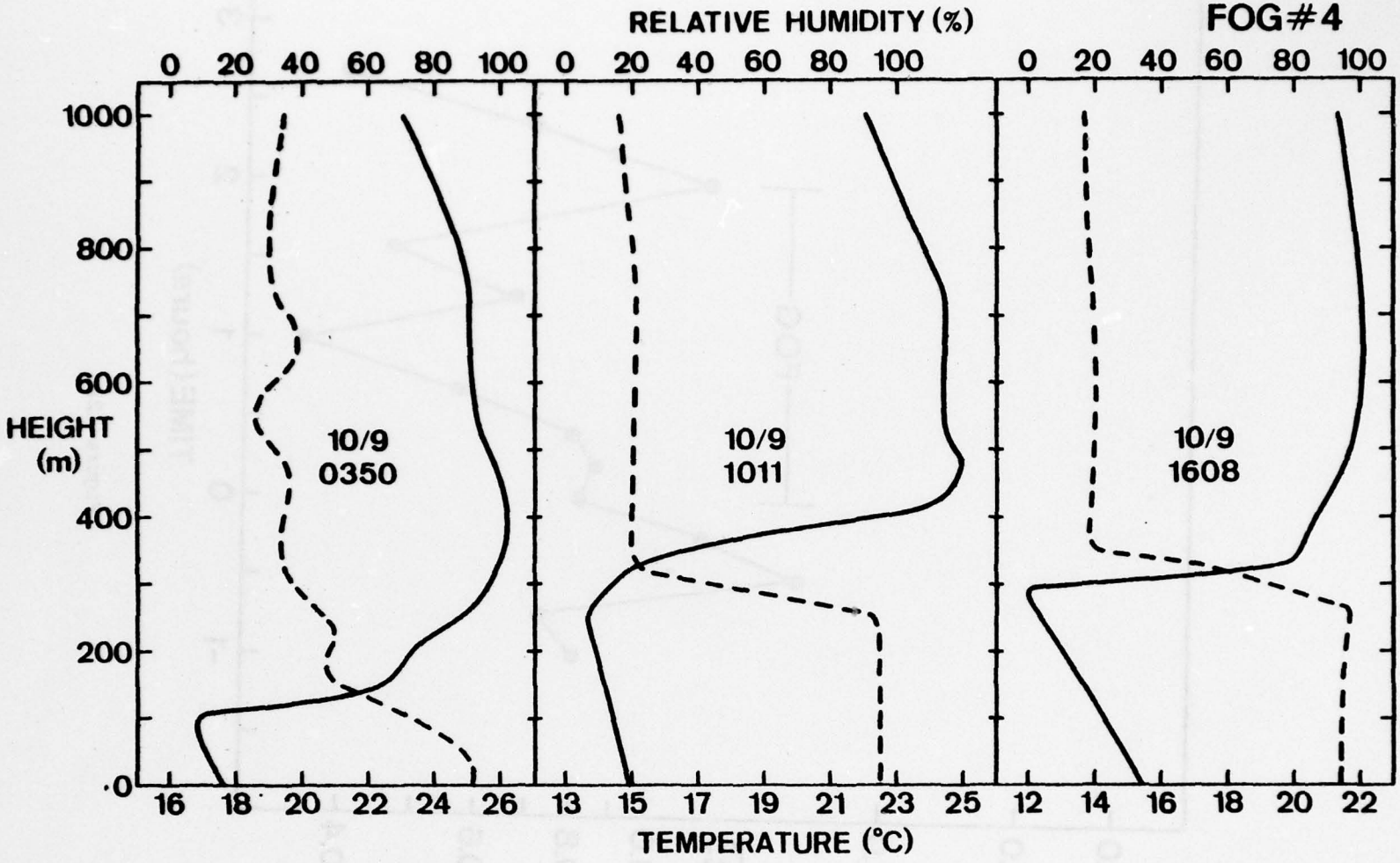
RELATIVE HUMIDITY (%)
FOG#4
0 20 40 60 80 100
0 20 40 60 80 100
0 20 40 60 80 100
1000
800
600
400
200
0
HEIGHT (m)
10/9 0350
10/9 1011
10/9 1608
16 18 20 22 24 26
13 15 17 19 21 23 25
12 14 16 18 20 22
TEMPERATURE (°C)

Figure 11d.

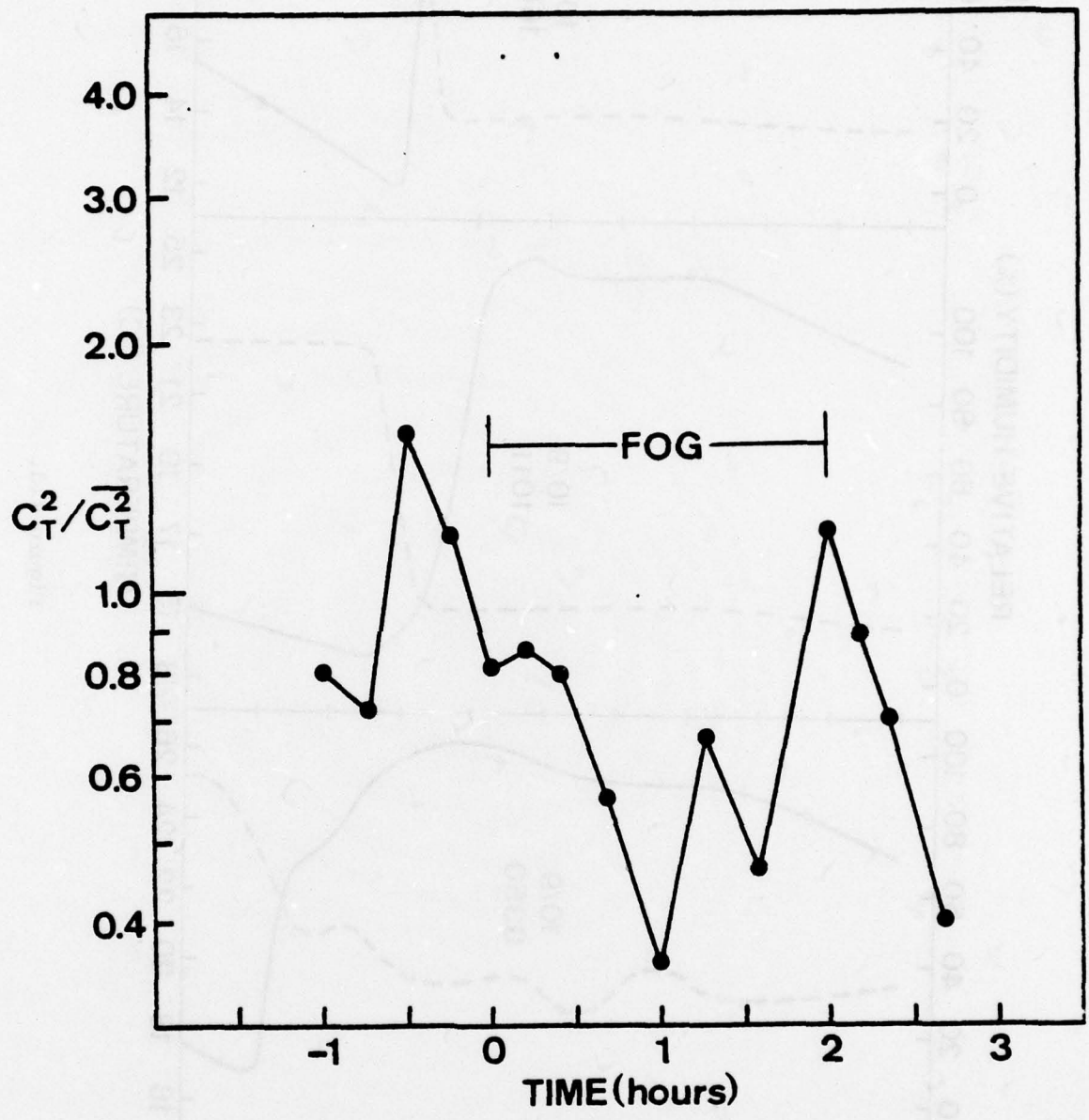

Figure 12a.

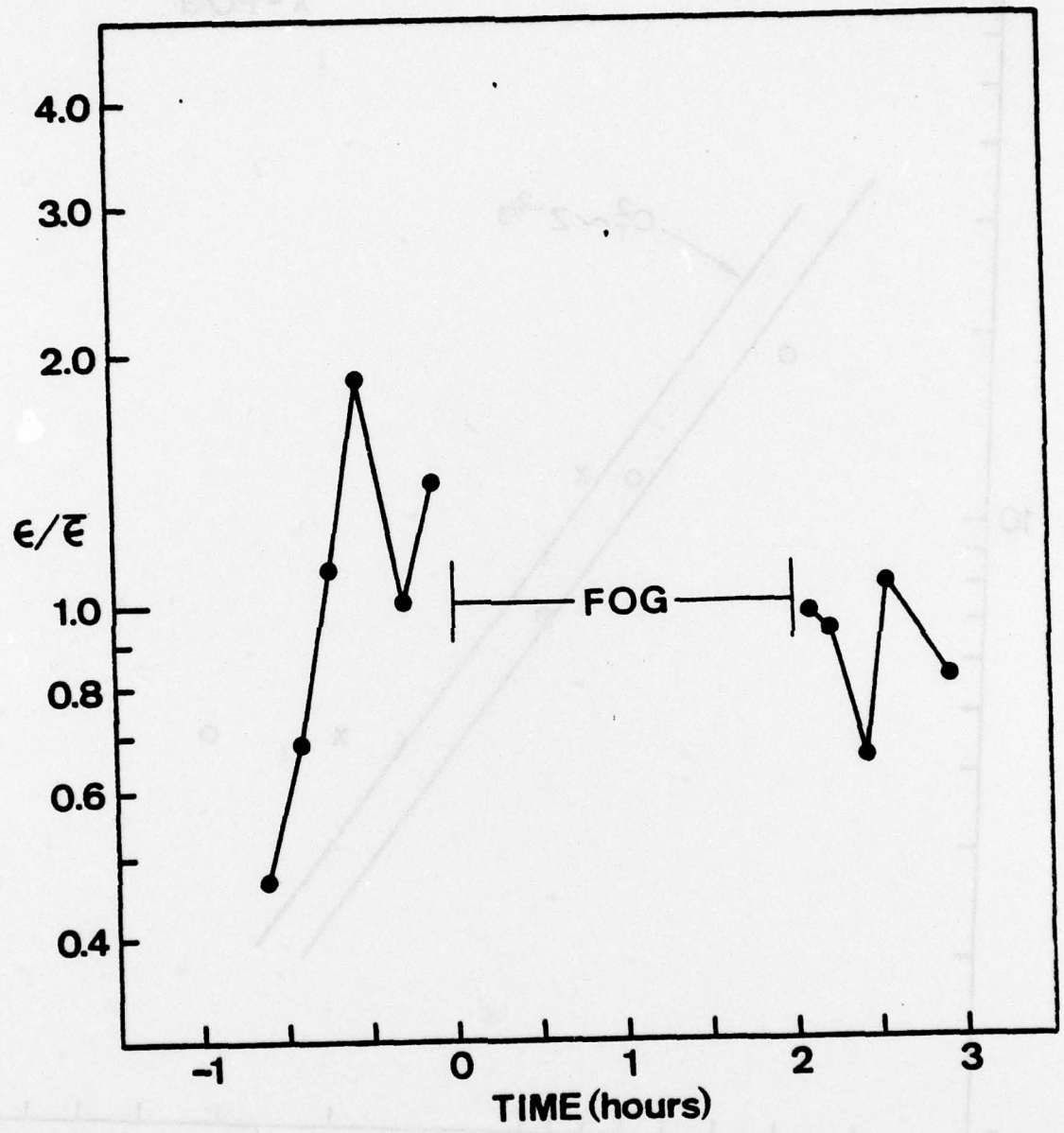

Figure 12b.

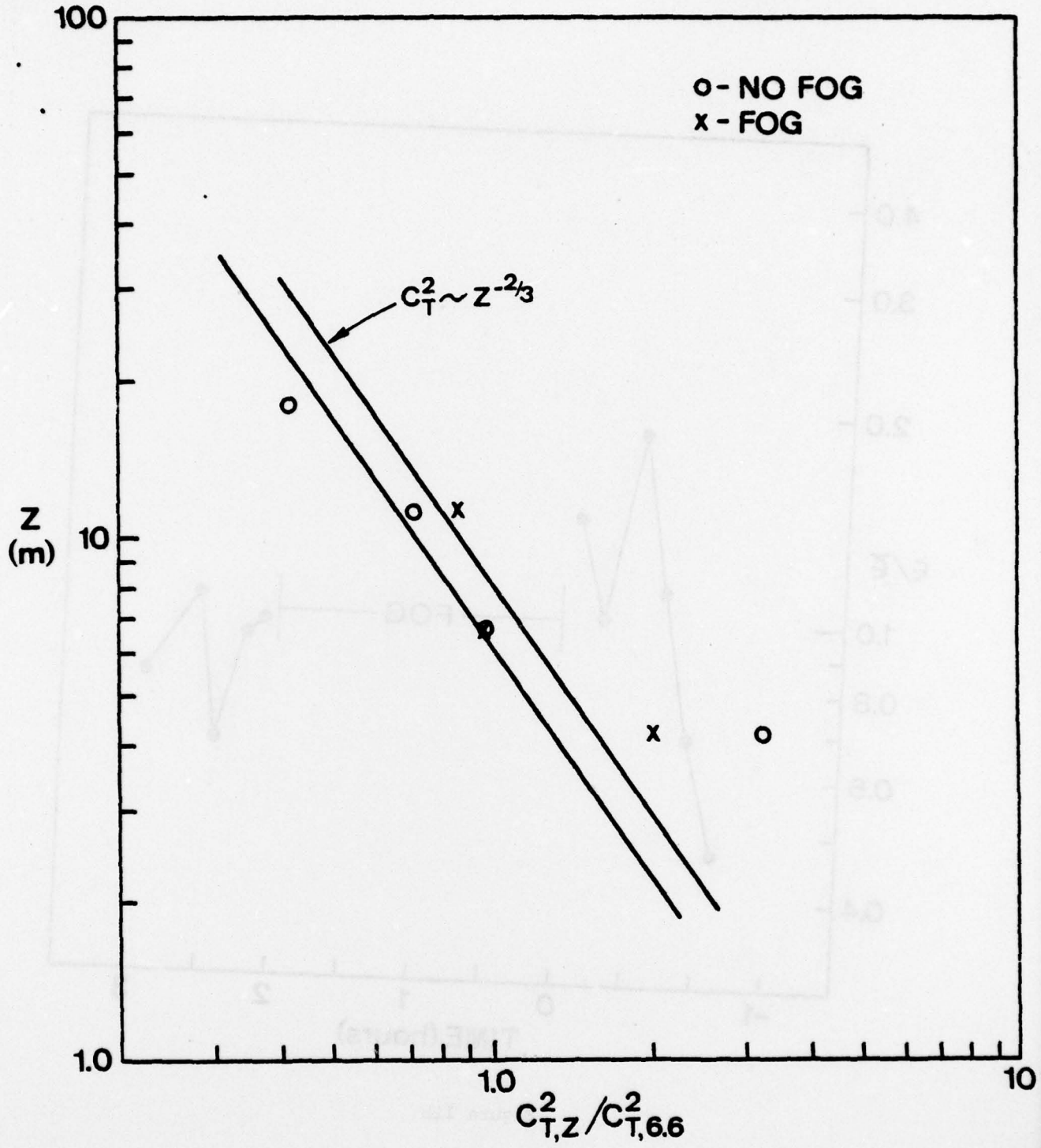

Figure 13.

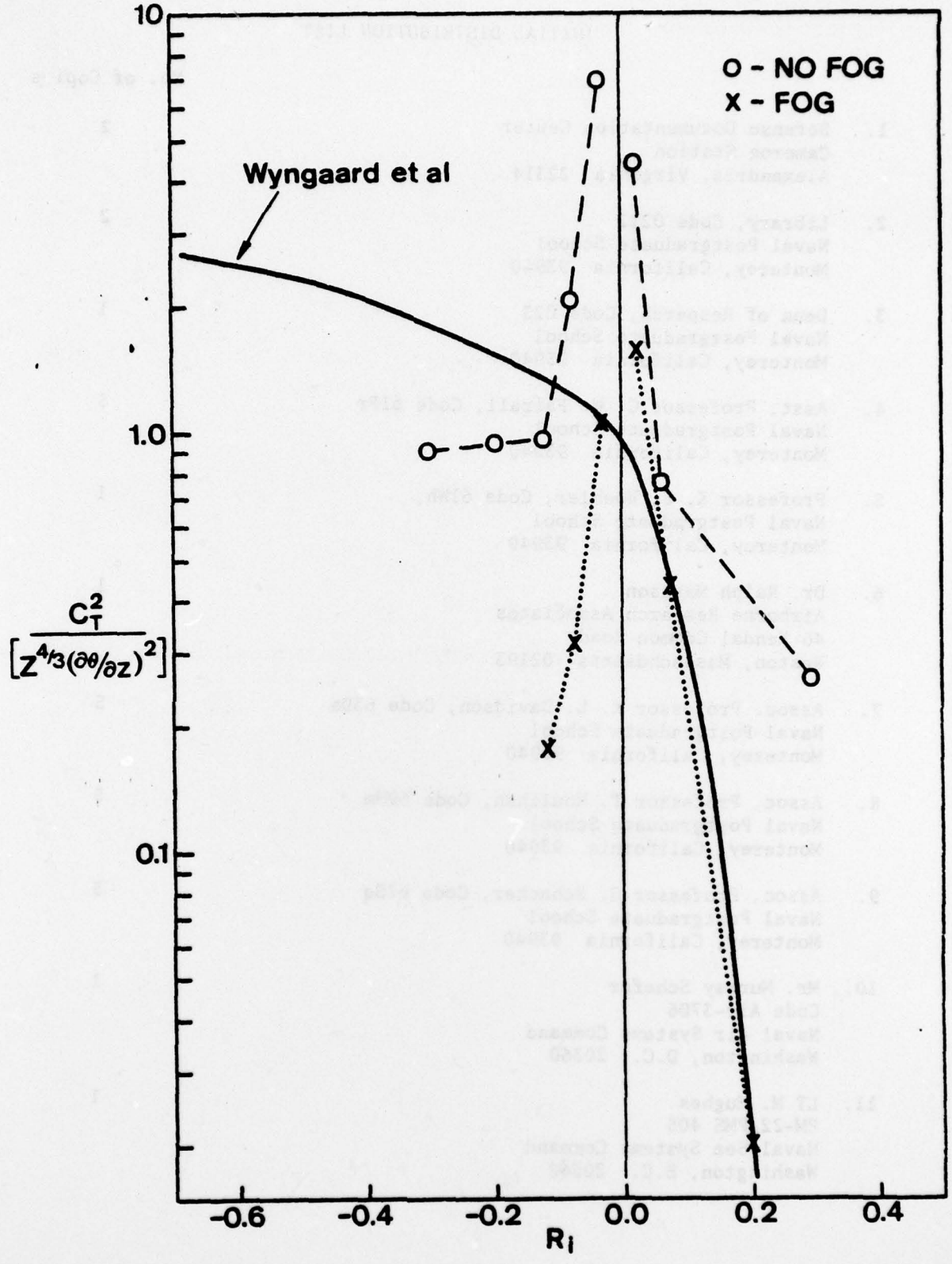
10
1.0
0.1
O - NO FOG
X - FOG
Wyngaard et al
$\frac{C_T^2}{[Z^{4/3}(\partial\theta/\partial z)^2]}$
-0.6
-0.4
-0.2
0.0
0.2
0.4
R_i

Figure 14.

INITIAL DISTRIBUTION LIST

		No. of Copies
1.	Defense Documentation Center Cameron Station Alexandria, Virginia 22314	2
2.	Library, Code 0212 Naval Postgraduate School Monterey, California 93940	2
3.	Dean of Research, Code 023 Naval Postgraduate School Monterey, California 93940	1
4.	Asst. Professor C. W. Fairall, Code 61Fr Naval Postgraduate School Monterey, California 93940	5
5.	Professor K. E. Woehler, Code 61Wh Naval Postgraduate School Monterey, California 93940	1
6.	Dr. Ralph Markson Airborne Research Associates 46 Kendal Common Road Weston, Massachusetts 02193	1
7.	Assoc. Professor K. L. Davidson, Code 63Ds Naval Postgraduate School Monterey, California 93940	5
8.	Assoc. Professor T. Houlihan, Code 69Hm Naval Postgraduate School Monterey, California 93940	5
9.	Assoc. Professor G. Schacher, Code 61Sq Naval Postgraduate School Monterey, California 93940	5
10.	Mr. Murray Schefer Code Air-3706 Naval Air Systems Command Washington, D.C. 20360	1
11.	LT M. Hughes PM-22/PMS 405 Naval Sea Systems Command Washington, E.C. 20362	1

12. Dr. Stuart Gatham 1
Code 8326
Naval Research Laboratory
Washington, D.C. 20375

13. Dr. Lothar Rohnke 1
Code 8320
Naval Research Laboratory
Washington, D.C. 20375

14. Dr. B. Katz 1
Naval Surface Weapons Center
White Oak
Silver Spring, Maryland 20910

15. Professor Dale Leipper, Code 68Lr 1
Naval Postgraduate School
Monterey, California 93940

16. Eugene J. Mack 1
Calspan Corporation
Buffalo, New York 14221